AFFDL-TR-77-117 FOR FURTHER TRAN

AN OPTIMIZATION STUDY FOR GENERATING SURFACE-ORIENTED COORDINATES FOR ARBITRARY BODIES IN HIGH-RE FLOW

TECHNOLOGY, INCORPORATED
DAYTON, OHIO 45431

UNIVERSITY OF DAYTON
DAYTON, OHIO 45469

DECEMBER 1977

TECHNICAL REPORT AFFDL-TR-77-117
Final Report for Period March 1976 – September 1976

AIR FORCE FLIGHT DYNAMICS LABORATORY
AIR FORCE WRIGHT AERONAUTICAL LABORATORIES
AIR FORCE SYSTEMS COMMAND
WRIGHT-PATTERSON AIR FORCE BASE, OHIO 45433

NOTICE

When Government drawings, specifications, or other data are used for any purpose other than in connection with a definitely related Government procurement operation, the United States Government thereby incurs no responsibility nor any obligation whatsoever; and the fact that the government may have formulated, furnished, or in any way supplied the said drawings, specifications, or other data, is not to be regarded by implication or otherwise as in any manner licensing the holder or any other person or corporation, or conveying any rights or permission to manufacture, use, or sell any patented invention that may in any way be related thereto.

This technical report has been reviewed and is approved for publication.

WILBUR L. HANKEY, JR, Ph.D.
Tech Mgr, Computational Aero Gr
Aerodynamics & Airframe Br

GUION S. BLUFORD, JR, Maj, USAF
Chief, Aerodynamics & Airframe Br
Aeromechanics Division

FOR THE COMMANDER

ALFRED C. DRAPER
Assistant for Research & Technology
Aeromechanics Division

"If your address has changed, if you wish to be removed from our mailing list, or if the addressee is no longer employed by your organization please notify Dr. W.L. Hankey, W-PAFB, OH 45433 to help us maintain a current mailing list".

Copies of this report should not be returned unless return is required by security considerations, contractual obligations, or notice on a specific document.

AIR FORCE/56780/24 March 1978 — 150

UNCLASSIFIED

SECURITY CLASSIFICATION OF THIS PAGE (When Data Entered)

REPORT DOCUMENTATION PAGE	READ INSTRUCTIONS BEFORE COMPLETING FORM
1. REPORT NUMBER: AFFDL-TR-77-117	2. GOVT ACCESSION NO. / 3. RECIPIENT'S CATALOG NUMBER
4. TITLE (and Subtitle): AN OPTIMIZATION STUDY FOR GENERATING SURFACE-ORIENTED COORDINATES FOR ARBITRARY BODIES IN HIGH RE-FLOW	5. TYPE OF REPORT & PERIOD COVERED: FINAL REPORT, MAR 76-SEP 76 / 6. PERFORMING ORG. REPORT NUMBER
7. AUTHOR(s): U. Ghia, University of Cincinnati; J.K. Hodge, AFFDL, WPAFB and W.L. Hankey, AFFDL, WPAFB	8. CONTRACT OR GRANT NUMBER(s): F33615-73-C-4155, F33615-76-C-3145
9. PERFORMING ORGANIZATION NAME AND ADDRESS: Technology, Incorporated, Dayton, Ohio 45431 and University of Dayton, Dayton, Ohio 45469	10. PROGRAM ELEMENT, PROJECT, TASK AREA & WORK UNIT NUMBERS: 61102F 2307 0418
11. CONTROLLING OFFICE NAME AND ADDRESS: Aeromechanics Division, Air Force Flight Dynamics Laboratory, WPAFB Ohio 45433	12. REPORT DATE: Dec 1977 / 13. NUMBER OF PAGES: 80
14. MONITORING AGENCY NAME & ADDRESS(if different from Controlling Office): N/A	15. SECURITY CLASS. (of this report): UNCLASSIFIED / 15a. DECLASSIFICATION/DOWNGRADING SCHEDULE

16. DISTRIBUTION STATEMENT (of this Report)

Approved for public release; distribution unlimited

17. DISTRIBUTION STATEMENT (of the abstract entered in Block 20, if different from Report)

18. SUPPLEMENTARY NOTES

Presented at the AIAA 3rd Computational Fluid Dynamics Conference at Albuquerque, New Mexico, June 1977.

19. KEY WORDS (Continue on reverse side if necessary and identify by block number)

Surface-Oriented Coordinates
Arbitrary Bodies
Boundary-Layer Dependent Mesh
Far-Field Boundary
Optimization of Numerical Transformation

20. ABSTRACT (Continue on reverse side if necessary and identify by block number)

The numerical coordinate-transformation technique for generating surface-oriented coordinates for arbitrary geometries is examined carefully in order to optimize the procedures involved, especially for high-Reynolds number flow. The areas studied include appropriate stretching of the viscous region while minimizing truncation error and optimum location of the far-field boundary for computational efficiency. Examination →

DD FORM 1 JAN 73 1473 EDITION OF 1 NOV 55 IS OBSOLETE

UNCLASSIFIED

SECURITY CLASSIFICATION OF THIS PAGE (When Data Entered)

of certain limiting forms of the nonlinear partial differential equations for the coordinates is found to lead to useful information about the behavior of the numerical solutions. It also enables the development of a simple procedure for formulating an improved starting solution for the nonlinear equations. Finally, an effort is made to maintain local near-orthogonality for the coordinates in the physical domain.

An implicit numerical method of solution, employing these optimization procedures, has led to reduction of the previously required computer time by an order of magnitude, for the cases examined.

FOREWORD

This research was performed while the first author, Dr. U. Ghia, of the University of Cincinnati, was a Visiting Scientist at the Flight Dynamics Laboratory, Wright-Patterson Air Force Base, under Government Contract No. F33615-73-C-4155 through Technology, Inc., and Government Contract No. F33615-76-C-3145 through the University of Dayton. The project, task and work unit numbers for this research are 61102F 2307 0418, with Dr. W.L. Hankey, FXM, as project engineer. The time period for this research project was March, 1976, through September, 1976.

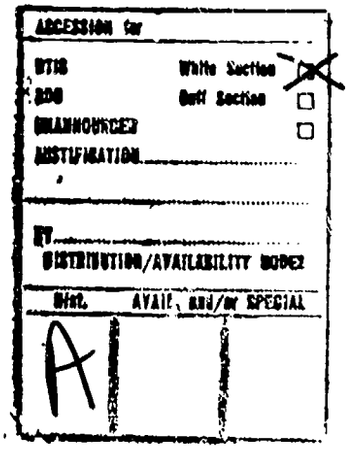

TABLE OF CONTENTS

LIST OF FIGURES

LIST OF TABLES

SECTION I

INTRODUCTION

The accurate solution of fluid dynamics problems of practical significance continues to comprise a challenging area of research owing to the complexity of the differential equations and boundary conditions encountered in the mathematical representation of these problems. At the same time, the demands placed on technology today require attacking problems of increasing complexity. Rapid advances in computing machines and the progress in the development of numerical algorithms now allow the consideration of some complex problems not heretofore solvable. However, the formulation of the problem itself has a very significant role in the success of its solution and in the efficiency with which the solution is obtainable. The emphasis on efficiency of a solution increases with the complexity of the problem as it can frequently make the difference between the practicality, or otherwise, of obtaining the solution of the problem.

An essential step in the proper formulation of the problem consists of the selection of an appropriate system of coordinates for representing the problem. In order for a coordinate system to be suitable, it must satisfy several fundamental requirements. Primary among these is the requirement that the coordinates be surface-oriented along all the boundaries of the problem, as this leads to simple and accurate expressions for the boundary conditions of the problem. For flow configurations with boundaries having analytical shapes, surface-oriented coordinates may be determined through analytical transformations. The technique of conformal transformations has been recently used very ingeniously

to formulate surface-oriented coordinates for some non-simple geometries. The procedure developed by Ives[1]* using a sequence of conformal transformations was later employed by Grossman and Melnik[2] to successfully compute the transonic flow over two-element airfoil systems. Moretti[3] has developed a transformation technique, consisting of repeated applications of a simple conformal mapping function, to generate surface-oriented coordinates for complex geometries, such as a typical airframe configuration.

Of course, it is always desirable to seek analytical transformation techniques rather than numerical transformations because, in the case of the former, the mapping as well as all coordinate-derivatives are defined exactly. Nevertheless, analytical transformations have certain inherent limitations. The conformal mapping technique, which has been so successful for two-dimensional transformations, is not defined for three-dimensional transformations. It can, however be used for a three-dimensional problem to determine surface-oriented two-dimensional coordinates in planes perpendicular to the third dimension in the problem. This approach is useful when the variations of the body geometry in this third dimension are only gradual. Thus, it is clear that, for general three-dimensional configurations as well as for arbitrary two-dimensional configurations, the more general numerical transformation techniques need

---

* Superscript numerals denote similarly numbered references at end of report.

to be investigated.

Considerable progress has been made in the development of numerical transformations for determining surface-oriented coordinates for complex configurations [e.g., Refs. 4 and 5, as well as the additional references listed therein]. While the fundamental procedure of these numerical transformations has been well-known for more than a decade, it has been given wide exposition only recently. Thompson et al.[4] employed the technique to formulate the coordinates for several external-flow configurations, involving doubly connected regions. Ghia et al.[5] developed the analysis for three-dimensional numerical transformations, with the cylindrical coordinate system as the starting system; for geometrical similarity with respect to the radial direction, the coordinate-transformation equations can be made to resemble those for the two-dimensional case.

The procedures developed are applicable to arbitrary geometries and, for two-dimensional configurations, consist, in principle, of solving elliptic equations of the form

$$\nabla^2 \eta = Q \quad , \qquad \nabla^2 \zeta = R \quad , \tag{1}$$

after expressing them in their inverted forms, i.e., with the roles of the independent and the dependent variables interchanged. The boundary conditions needed for a unique solution of Equation (1) consist of specified distributions of mesh points along all boundaries of the solution domain. In Equation (1), the symbol η denotes the transverse coordinate, and ζ denotes the coordinate along the surface [Figure 1]. The forcing functions Q and R

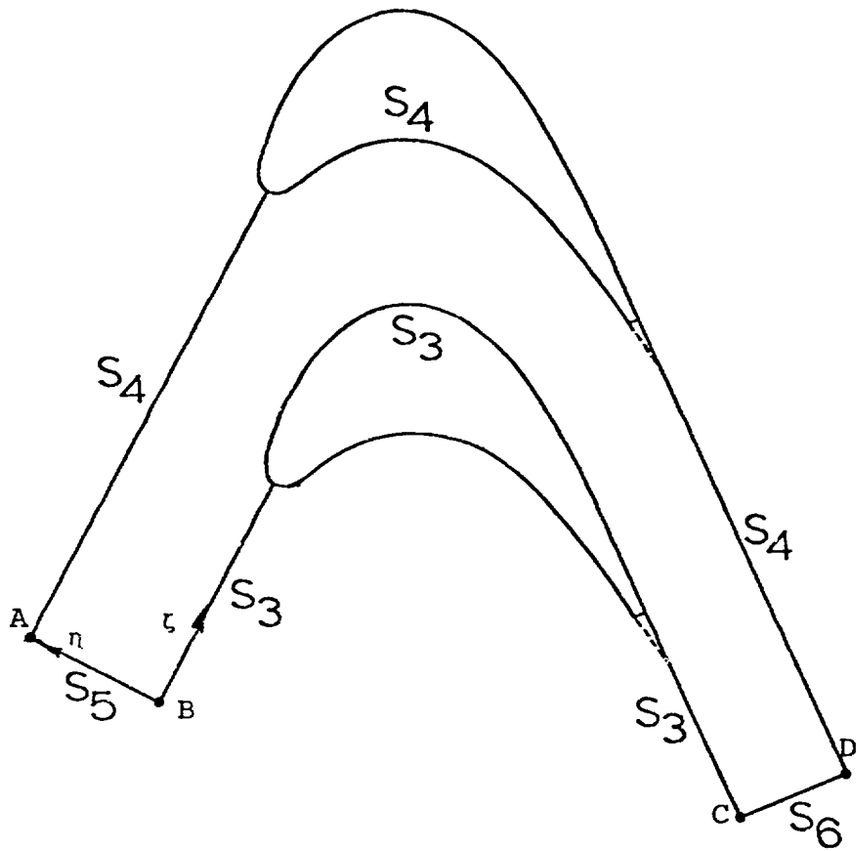

FIG. 1. SCHEMATIC REPRESENTATION OF ARBITRARY GEOMETRICAL CONFIGURATION - PHYSICAL PLANE

serve to control the coordinate spacing in the interior of the physical domain. The resulting solution can provide a more optimum distribution of a given number of mesh points than would be possible with a conformal coordinate system using $Q \equiv R \equiv 0$. In the computational domain, the transformed coordinates are rectangular and uniformly spaced.

While the basic procedure is quite well understood, the transformation involves several areas of detail that need to be refined and formalized. For example, considerations of accuracy of the flow solution require that regions of large flow gradients be appropriately stretched in the computational domain. This is to be achieved by employing the proper form, in magnitude and sign, for the forcing functions in the coordinate equations. Although it is simple to establish the signs of the forcing functions, the magnitudes used for the forcing functions, in order to achieve a desired mesh-point distribution, are frequently determined by a process of trial and error. It is necessary to develop a systematic procedure for determining the forcing function needed to provide the required spacing of the coordinate lines. Moreover, when a nonuniform grid is desired in the physical domain, the distribution of points along the boundaries, prescribed as boundary conditions, must be consistent with the forcing functions used for the solution in the interior. Failure to maintain this consistency may lead to coordinates that exhibit discontinuities in their derivatives near the boundaries.

Another area requiring further study deals with the question of the location of the far-field boundary for subsonic external flow past a body. One answer to this question consists of locating

the far-field boundary infinitely far from the body. However, this necessitates the use of an analytical transformation to map the unbounded physical domain to a finite region. To the best knowledge of the authors, this has not been done so far for arbitrary bodies, in conjunction with a numerical transformation. Frequently, the approach used for locating the far-field boundary for flow past a body has consisted of repeating the calculations with two or more different far-field-boundary locations until the resulting differences in the normal or tangential stress distributions on the body surface are within a certain prescribed limit. As discussed later in the present study, this process may not be necessary, especially for the commonly studied bodies such as circular cylinders, airfoils, etc.

It is also necessary to recall that the basic approach for numerical generation of surface-oriented coordinates does nothing to maintain or ensure orthogonality for the new coordinates. However, the use of an orthogonal or near-orthogonal coordinate system is often advantageous as regards convergence rate of the numerical scheme. An orthogonal system is also desirable if one intends to make a direction-related approximation in the flow equations, e.g., parabolization with respect to the streamwise direction, at least in the viscous region near the body surface. Therefore, it would be desirable to develop a procedure for orthogonalization of a given numerical non-orthogonal coordinate system. This may be included as an optional step at the end of the main solution procedure.

The purpose of the present study is to optimize the numerical transformation procedure for determining a suitable system of

surface-oriented coordinates for arbitrary geometrical configurations. The resulting coordinates are required to provide appropriate stretching of the viscous region near the body surface, in the computational domain, so as to be suitable for high-Reynolds-number flow calculations. It is also desired that the coordinates be nearly orthogonal in the physical domain, at least near the boundaries. Attempt is made to provide as much formalism to the procedure as possible, so as to maintain versatility and generality for application and minimize the need for a trial-and-error approach. At the same time, this should not be interpreted as de-emphasizing the significance of good engineering intuition in the efficient solution of a practical problem. In addition to analyzing those aspects of the transformation discussed in the preceding paragraphs, effort is also made to improve the numerical scheme itself. The major steps used to achieve the objectives of this research are discussed in the following sections of this report.

SECTION II

DESCRIPTION OF BASIC PROCEDURE FOR NUMERICAL GENERATION OF SURFACE-ORIENTED COORDINATES

In order to provide the proper perspective for the optimization steps to be discussed in this report, a brief description is first given of the basic procedure for numerical generation of surface-oriented coordinates for arbitrary geometries. The analysis presented here is for two-dimensional geometries or for cylindrical geometries with radial similarity. Therefore, in the physical domain, the configuration is represented in terms of the coordinates (ϕ, z) such that

$$\phi = \begin{cases} y & \text{for two-dimensional configurations} \\ r\theta & \text{for cylindrical configurations.} \end{cases}$$

Nevertheless, all steps in the analysis are either applicable or extendable to three-dimensional transformations.

In principle, the numerical transformation procedure consists of determining the boundary-oriented transformed coordinates as the solutions of the following Poisson equations:

$$\eta_{\phi\phi} + \eta_{zz} = Q \tag{2}$$

and

$$\zeta_{\phi\phi} + \zeta_{zz} = R \tag{3}$$

where η, ζ are the transformed surface-oriented coordinates;

ϕ, z are the physical coordinates;

Q, R are continuous functions of (η, ζ) or (ϕ, z), specified so as to provide desired control on the coordinate distribution.

The boundary conditions for Equations (2) and (3) must be specified on the basis of the particular geometry under consideration. For non-simple geometries, they will generally not be along constant values of ϕ or z.

Therefore, it is necessary to derive a set of equations equivalent to Equations (2) and (3), such that only η, ζ appear as independent variables. This has been done previously[4,5] and results in the following 'inverted' equations:

$$a\,\phi_{\eta\eta} + 2b\,\phi_{\eta\zeta} + c\,\phi_{\zeta\zeta} + J^2(Q\,\phi_\eta + R\,\phi_\zeta) = 0 \qquad (4)$$

and

$$a\,z_{\eta\eta} + 2b\,z_{\eta\zeta} + c\,z_{\zeta\zeta} + J^2(Q\,z_\eta + R\,z_\zeta) = 0 \qquad (5)$$

where

$$a = \phi_\zeta^2 + z_\zeta^2 \quad ,$$

$$b = -(\phi_\eta\phi_\zeta + z_\eta z_\zeta) \quad ,$$

$$c = \phi_\eta^2 + z_\eta^2 \qquad (6)$$

and $$J = \phi_\eta z_\zeta - \phi_\zeta z_\eta \quad . \qquad (7)$$

It is noted that the quantity J defined by Eq. (7) is exactly the Jacobian of the coordinate-transformation.

The boundary conditions for Equations (4) and (5) can now be specified as the prescribed values of ϕ and z, along the boundaries $\eta=\eta_1$, η_2 and $\zeta=\zeta_1$, ζ_2 ; [see Figure 2]. However, when a non-uniform spacing of the transformed coordinates is desired in the physical plane, the boundary-values of ϕ and z

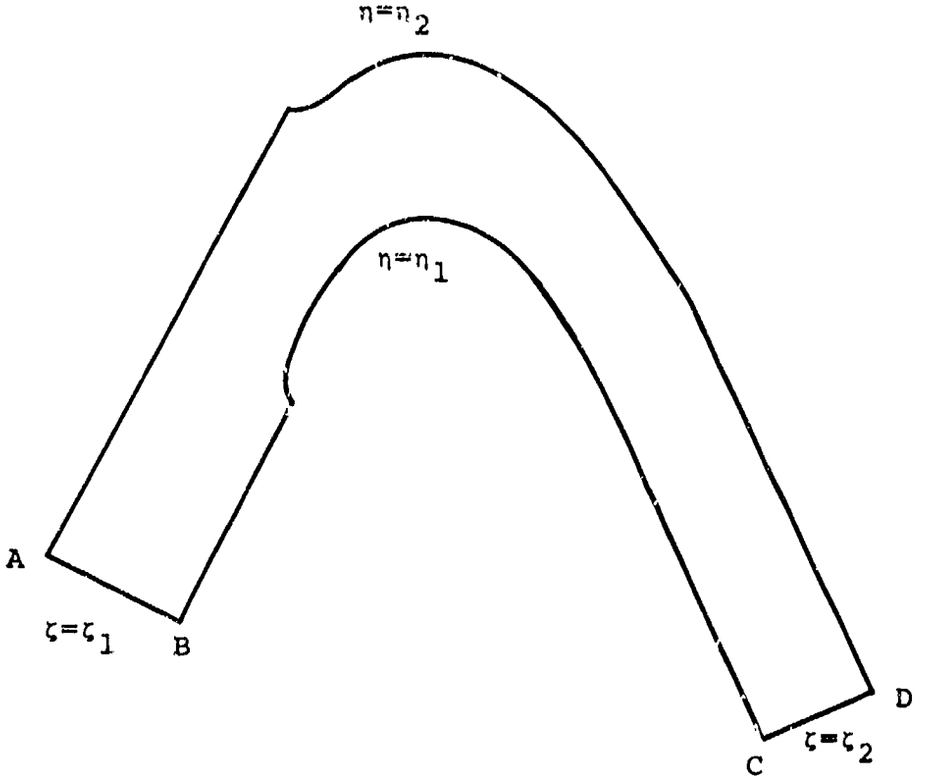

FIG. 2. REPRESENTATION OF BOUNDARIES OF ARBITRARY GEOMETRICAL CONFIGURATION.

may no longer be prescribed independent of the forcing functions Q and R used in Eqns. (4) and (5). Until now, the situation was handled by giving up the Dirichlet boundary conditions for Eqns. (4)-(5), in favor of Neumann boundary conditions consisting of zero normal gradients of ϕ and z at the boundaries. The drawback of this approach, as well as the present improved approach for treating this and several other aspects of the general transformation procedure, are discussed next. It is important to note that improvement in the analysis also leads, frequently, to improvements in the finite-difference method for the numerical solution of the transformation equations.

SECTION III

OPTIMIZATION OF NUMERICAL COORDINATE-TRANSFORMATION PROCEDURE

1. REPRESENTATION OF VISCOUS REGION NEAR BODY OR OTHER HIGH-GRADIENT REGIONS

As the Reynolds number Re for a flow problem increases, the thickness of the viscous region near the body surface decreases, so that the flow variables exhibit large transverse gradients in this important region. Therefore an accurate computation of the flow solution requires that this region be appropriately stretched in the transformed domain so as to provide a reasonable number of computational points within this region. As mentioned in Section 1, this is achieved by using the proper form for the function Q in the coordinate-transformation equations. The proper sign for Q can generally be determined on the basis of the theory of harmonic functions. However, no formal theory is available for determining the magnitude of Q. It is only known that the magnitude required for Q generally increases with the degree of stretching required and, hence, with increasing Re. A procedure has been developed, in the present work, for determining $Q(\eta)$ such that a prescribed number of computational points are located in a Blasius boundary layer at a body surface. Before describing this procedure, it is necessary to consider some of the adverse effects of the use of a non-zero Q on the computational efficiency of the solution of the coordinate-transformation equations. As the following analysis and discussion shows, most of these adverse effects have been minimized in the present work. In fact, the analysis has shed light on some very useful aspects of the probler..

a. Boundary Conditions for Coordinate Transformation with Forcing Function

It had been observed that the convergence rate of the coordinate solution was usually retarded by the use of a non-zero Q, even if only moderate magnitudes were used for Q. One of the causes for this seems to be the following. In order to avoid discontinuities in the transformed-coordinate derivatives, it is necessary that the distribution of points along the end boundaries AB and CD [Fig. 1] be consistent with the function Q used in the interior. The method used so far to achieve this consisted of specifying conditions only on the coordinate derivatives rather than on the locations of the points along AB and CD. This leads to slower convergence rate for the solution, especially if an explicit numerical scheme is employed. Moreover, when derivative boundary conditions were used at both boundaries AB and CD, the solution was sometimes reported[6] to violate the maximum principle, resulting in cross-over of the coordinates.

In the present work, use is made of the limiting form of the coordinate equationsat the end-boundary (e.g., AB) to determine, prior to the complete solution, the point-distribution at this boundary, consistent with the Q used in the interior. The end boundary is generally a straight line, though not necessarily a vertical straight line. However, the required point-distribution may be determined for a vertical line and then transformed to yield the distribution along a general line such as A'B'.

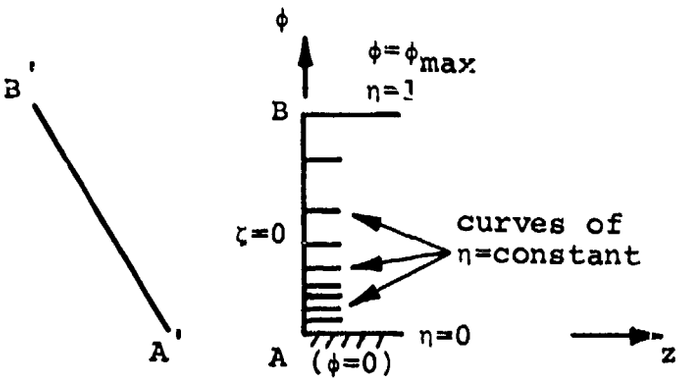

FIG. 3. TREATMENT OF BOUNDARY CONDITIONS ALONG A STRAIGHT BOUNDARY.

Along the boundary AB, where ζ=constant, the coordinate equations (1) reduce to

$$\eta_{\phi\phi} = Q(\eta) \tag{8}$$

if the $(\eta-\zeta)$ system is required to be orthogonal along AB. Since Q will not, in general, be a simple linear function of η, Eqn. (8) cannot be integrated directly. However, in its inverted form, this equation becomes

$$\phi_{\eta\eta} + Q\,\phi_{\eta}^{3} = 0 \tag{9}$$

with the boundary conditions

$$\phi(0) = 0 \; ; \quad \phi(1) = \phi_{max} \; . \tag{10}$$

Equation (9) is a nonlinear differential equation for ϕ, with a varying coefficient, and can be easily solved numerically, using the boundary conditions (10). A simple tridiagonal scheme, with linearization or quasi-linearization of the term ϕ_{η}^{3}, was used

to solve this equation, with the nonlinearity being restored through an iterative procedure. Figure 4 shows the solution, hence the point-distribution along AB, obtained with $Q(\eta)$ given by the following analytical form:

$$Q(\eta) = \sum_{k=1}^{2} \frac{1}{a_k} \exp[-(\eta-\eta_k)^2/(2b_k^2)] \tag{11}$$

where $a_1 < 0$, $|a_1| = a_2$,

$b_1 = b_2 = 0.1$,

$\eta_1 = 0$,

$\eta_2 = 1$. (12)

This form for $Q(\eta)$ provides a fine mesh near η_1 as well as near η_2.

The resulting distribution is then transformed to a corresponding distribution along line A'B' such that incremental distances along A'B' are the same as the corresponding increments along AB. Thus, between the two points i and (i+1),

$$ds^2 = (\bar{\phi}_{i+1} - \bar{\phi}_i)^2 = (\phi_{i+1} - \phi_i)^2 + (z_{i+1} - z_i)^2 \tag{13}$$

where $\bar{\phi}$ denotes the solution of Equation (9) along AB. Denoting the slope of line A'B' by m, Equation (13) can be rewritten as

$$(\bar{\phi}_{i+1} - \bar{\phi}_i)^2 = (1 + m^2)(z_{i+1} - z_i)^2 \tag{14}$$

where $m = (\phi_{i+1} - \phi_i)/(z_{i+1} - z_i)$.

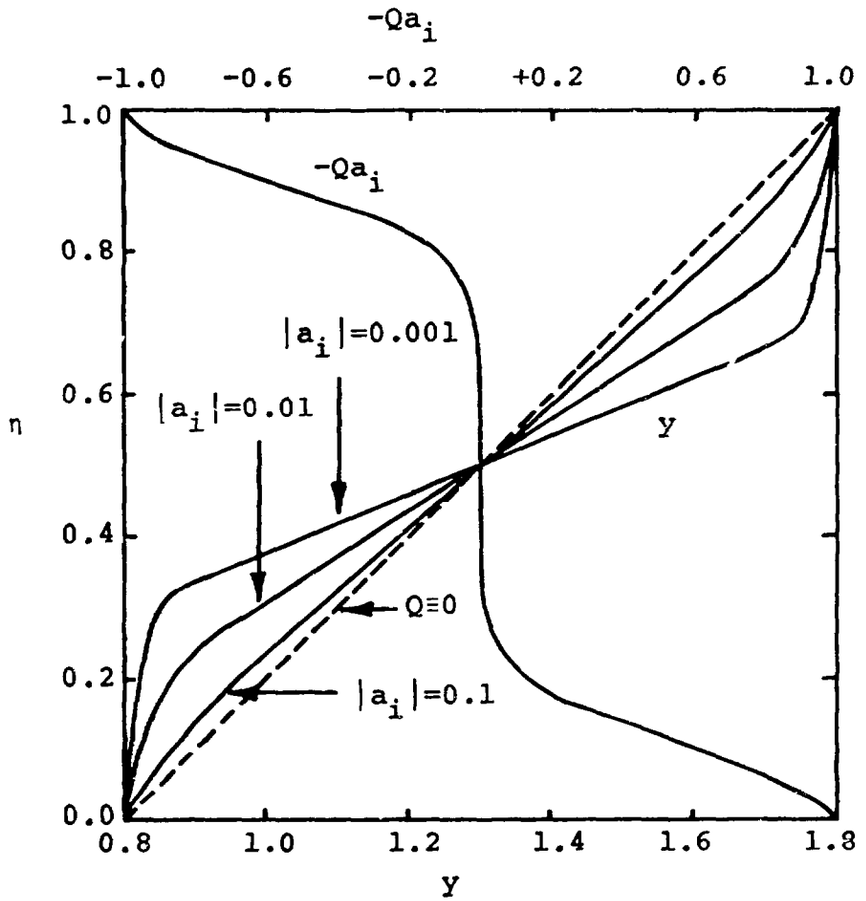

FIG. 4, SOLUTION OF $\phi_{\eta\eta} + Q\,\phi_\eta^3 = 0$ WITH Q(η) AS GIVEN BY EQ. (11).

Equation (14) yields the z-coordinates of the required point-distribution along the actual end-boundary A'B' as

$$z_{i+1} = z_i \pm \frac{1}{\sqrt{1+m^2}} \left(\bar{\phi}_{i+1} - \bar{\phi}_i\right) \tag{15}$$

where the sign to be used depends upon the sign of m. If $m > 0$, the positive sign must be used, while the negative sign is needed if $m < 0$. Therefore, Eq. (15) must be represented as follows:

$$z_{i+1} = z_i + \left\{\frac{m}{|m|}\right\} \frac{\left(\bar{\phi}_{i+1} - \bar{\phi}_i\right)}{\sqrt{1+m^2}} \quad . \tag{16}$$

Thereafter, ϕ_{i+1} may be determined from the slope m as

$$\phi_{i+1} = \phi_i + m(z_{i+1} - z_i) \quad . \tag{17}$$

Thus, starting with the coordinates of A', the value of ϕ and z for the required points along A'B' can be computed using the solution of Equation (9) and the relations (16)-(17). It must be noted that, if $m = 0$, Eqns. (16) and (17) must be replaced by

$$z_{i+1} = z_i + \left(\bar{\phi}_{i+1} - \bar{\phi}_i\right) \quad ,$$

$$\phi_{i+1} = \phi_i \quad . \tag{18}$$

Also, if $m \to \infty$, the proper relations are

$$z_{i+1} = z_i \quad ,$$

$$\phi_{i+1} = \phi_i + \left(\bar{\phi}_{i+1} - \bar{\phi}_i\right) \quad . \tag{19}$$

It is important that the length of AB along which Eqn. (9) is solved must be exactly equal to the length of the actual boundary A'B'. If this is not maintained, the nonlinearity of Eqn. (9) leads to a point-distribution along A'B' that corresponds to an effective function Q', whose values are related to Q by the square of ratio of the lengths of AB and A'B'.

b. Determination of Forcing Function from Specified Dirichlet Boundary Conditions

In another situation, the distribution of the points along the boundaries of an arbitrary geometrical configuration may be prescribed on the basis of some independent physical considerations for the flow problem. In order to obtain the transformed coordinates satisfying these boundary conditions, it is now necessary to determine the forcing function, which is consistent with the specified boundary-point distribution. In doing so, it is also desirable to maintain local orthogonality for the coordinates. Though applicable in general, the procedure described below discusses the determination of the forcing function R in Eqn. (3) from a known point-distribution along the surface η=constant.

Using the condition for local orthogonality (see Appendix A), i.e.,

$$\phi_\eta \phi_\zeta + z_\eta z_\zeta = 0 \quad , \tag{20}$$

the transformation equations (4-7) can be written as

$$a\,\phi_{\eta\eta} + c\,\phi_{\zeta\zeta} + J^2(Q\,\phi_\eta + R\,\phi_\zeta) = 0 \qquad (21)$$

and

$$a\,z_{\eta\eta} + c\,z_{\zeta\zeta} + J^2(Q\,z_\eta + R\,z_\zeta) = 0 \quad . \qquad (22)$$

At the surface η=constant, all derivatives with respect to ζ are easily evaluated from the given point-distribution. Therefore, if the η-derivatives appearing in the transformation equations can be estimated along this surface, then these equations can be used as algebraic equations for the forcing functions. For a reasonably fine grid in the η-direction, as would normally be used in a viscous region near the surface η=constant, it appears reasonable to assume that

$$z_{\eta\eta} \approx 0 \quad . \qquad (23)$$

A good estimate of ϕ_η and $\phi_{\eta\eta}$ is obtained by linear interpolation between their corresponding values at the end-boundaries where these quantities are known from the specified boundary-points. Finally, z_η is determined from the orthogonality condition (20) as

$$z_\eta = -\phi_\eta\phi_\zeta/z_\zeta \quad . \qquad (24)$$

With all the coordinate derivatives evaluated along the surface, Q is eliminated between Eqns. (21) and (22) to yield the following expression for R:

$$R = \frac{1}{J^2(\phi_\eta z_\zeta - \phi_\zeta z_\eta)} - [az_\eta\phi_{\eta\eta} + c(z_\eta\phi_{\zeta\zeta} - \phi_\eta z_{\zeta\zeta})] \quad . \qquad (25)$$

The denominator in Eqn. (25) has intentionally not been represented as J^3 in order to admit the possibility of employing different finite-difference representations for the derivatives in J^2 and in $(\phi_\eta z_\zeta - \phi_\zeta z_\eta)$ in Eqn. (25). This will be discussed further in the next section.

Thus, the function R can be determined at both boundaries represented by $\eta=\eta_1$ and $\eta=\eta_i$. Denoting these values of R by $R_1(\zeta)$ and $R_2(\zeta)$, the complete function $R(\eta,\zeta)$ to be used in the interior may be determined as

$$R(\eta,\zeta) = R_1 + (R_2 - R_1)\, f(\eta) \tag{26}$$

where $f(\eta)$ is a normalized monotonic continuous function of η, used to provide a smooth variation for R in the solution domain. If the forcing function Q is known and is monotonic with respect to η, then $f(\eta)$ may be chosen as

$$f(\eta) = \frac{Q(\eta,\zeta) - Q_1}{Q_2 - Q_1} \quad . \tag{27}$$

Another suitable choice for $f(\eta)$ consists of the sine function or the exponential-sine function.

This approach has been used to determine the function R from the specified distribution of points along the boundaries. The resulting solution for the transformed coordinates confirms that the required consistency has been properly maintained between the boundary conditions and the forcing functions.

c. Effect of Increasing Magnitude of Forcing Function on Solution Convergence Rate

It has been reported that the use of very large magnitudes for the forcing functions leads to numerical difficulties in terms of instabilities and oscillations. However, forcing functions of large magnitudes become necessary when a highly non-uniform coordinate spacing is required, such as in a boundary layer for a high-Re flow. A solution to this situation frequently consisted of obtaining the required coordinates by approaching the large forcing functions in a stepwise increasing manner. In the present work, it became possible to analyze the cause of this adverse numerical behavior by examining the limiting form of the inverted equations at the boundaries. In its simplest form, this limiting equation is given by Eqn. (9) for a vertical straight-line boundary represented by ζ=constant. Figure 5 shows the solution of Eqn. (9) for increasing values of $Q(\eta)$ as given by Eqn. (12), with ϕ_{max} equal to the length of the boundary AB in Fig. 1. Second-order accurate central finite-differences have been used to represent all derivatives in order to obtain these solutions.

It is seen from Fig. 5 that a satisfactory solution is obtained with $|Q|_{max} \leq 10^3$. For $|Q|_{max} \geq 10^4$, the solution begins to violate the maximum principle and shows a clear oscillatory behavior for $|Q|_{max} = 10^5$. It must be noted that this oscillatory solution is truly the correct converged solution of the finite-difference equation used. This behavior is due, in principle, to the increasing stiffness of Eqn. (9) with increase in Q. The situation may be remedied in one of two

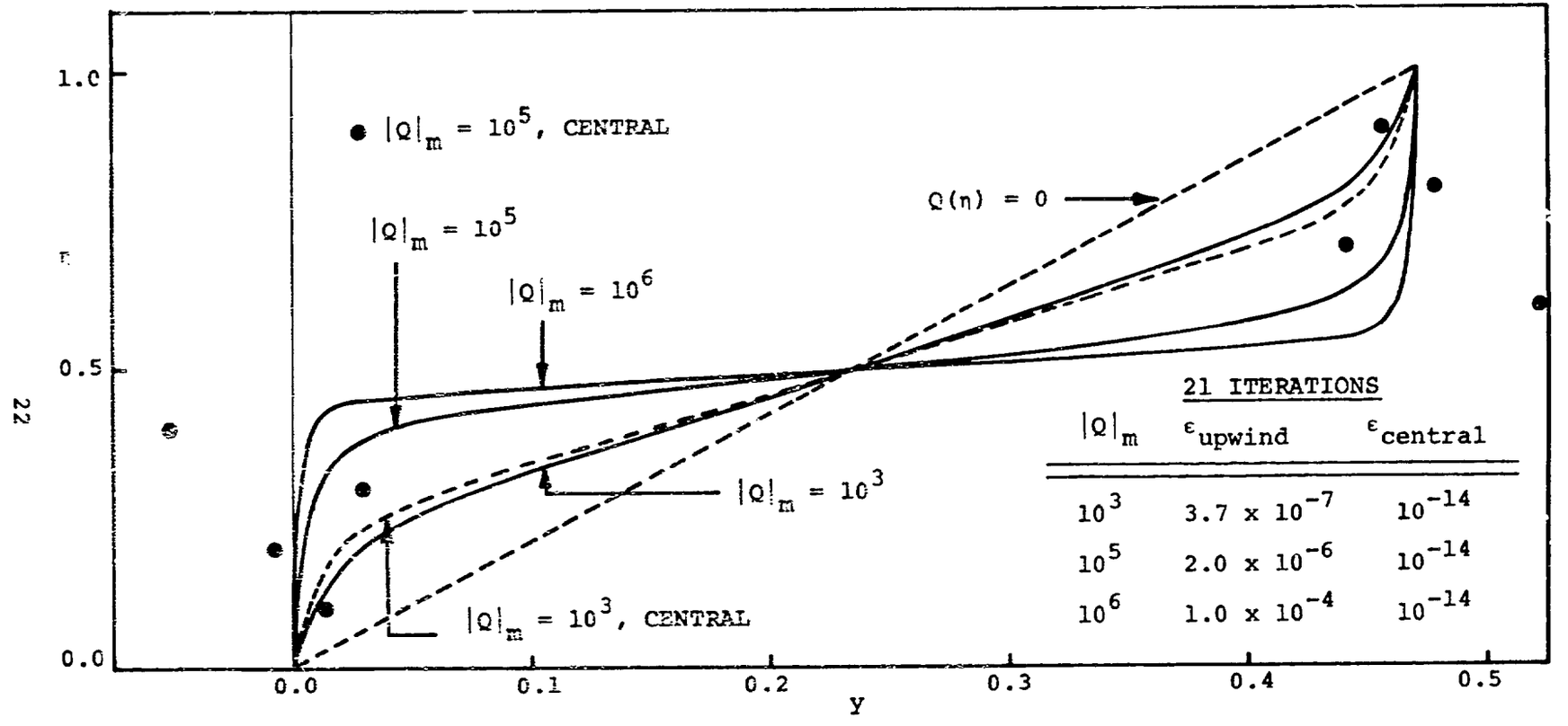

FIG. 5. EFFECT OF UPWIND DIFFERENCING AND CENTRAL DIFFERENCING ON SOLUTION OF LIMITING EQUATION FOR COORDINATES

ways:[7] the use of a finer mesh in the transformed coordinate η or the use of directional differencing. The use of a finer mesh leads to an increase in the computer storage and time required for the solution of the complete coordinate equations (4-7). Therefore, the use of directional or upwind differences is adopted here to obtain the proper solution, with large Q. For this purpose, Eqn. (9) is represented in its linearized form as

$$\phi_{\eta\eta} + C_1 \phi_\eta = 0 \tag{28}$$

and

$$C_1 = Q \phi_\eta^2 \quad . \tag{29}$$

The term ϕ_η in Eqn. (29) is represented by a central-difference approximation, while ϕ_η in Eqn. (28) is represented by an upwind difference such that a backward/forward difference is used when C_1 is negative/positive. This is easily accomplished by the following generalized representation:

$$C_1 \phi_\eta = (1-u)\, C_1 \phi_{\eta_C} + \frac{u}{2} [C_1^+ \phi_{\eta_F} + C_1^- \phi_{\eta_B}] \tag{30}$$

where $u = \begin{cases} 0 & \text{if central differencing is to be used,} \\ 1 & \text{for upwind differencing;} \end{cases}$

$$C_1^\pm = C_1 \pm |C_1| \quad ,$$

and ϕ_{η_C}, ϕ_{η_F}, ϕ_{η_B} denote two-point central-, forward- and backward-difference representations, respectively, of ϕ_η. Figure 5 shows the effect of using upwind differencing in the solution of Eqn. (28). With $|Q|_{max}$ in the range where an

acceptable central-difference solution was not obtainable, upwind differencing leads to a completely well-behaved solution. Some differences are also observed in the two solutions even for $|Q|_{max} = 10^3$, when an acceptable central-difference solution was readily obtainable. Because of the second-order accuracy of the central-difference solution, versus the first-order accuracy of the upwind-difference solution, the former may be preferred. However, the usefulness of upwind differencing, with large Q, indicates a more general applicability of the upwind-difference scheme.

In working with this limiting equation (28), it was also observed that the central-difference scheme converged very efficiently, even when the resulting solution was not monotonic. For those values of Q for which the limiting equation (9) leads to a non-monotonic solution, the solution of the full equations (4-7) exhibits instabilities when central differences are used for all the derivatives. On the other hand, upwind differencing led to an acceptable solution very efficiently, even though the convergence criterion was not satisfied. Efforts were made to improve the convergence properties of the solution by employing quasi-linearization in Eqn. (9), i.e., by representing it as

$$\phi_{\eta\eta} + (3Q\ \phi_{\eta}^{2})\phi_{\eta} - (2Q\ \phi_{\eta}^{3}) = 0 \qquad (31)$$

where the quantities in parentheses are evaluated at a previous iteration. Quasilinearization was found to increase the convergence rate of the central-difference scheme, but had little influence on the upwind scheme. The following table summarizes

the effect of the difference scheme on the convergence behavior of the solution.

	Error (ϵ) after 20 Iterations of Quasilinearized Equation (31)	
$\lvert Q\rvert_{max}$	Upwind	Central
10^3	10^{-7}	10^{-14}
10^5	10^{-6}	10^{-14} - oscillatory solution
10^6	10^{-4}	

The error was defined as $\epsilon = \sum_{i=1}^{IMAX} |\phi_i^{n+1} - \phi_i^n|$ where n denotes iteration number. It should be pointed out that, even with $\epsilon = 10^{-4}$, the upwind-difference solution was a completely acceptable solution for ϕ. Therefore, it appears that appropriate use of upwind differencing constitutes an efficient scheme for the solution of the complete transformation equations (4-7) also. In the interior of the solution domain, it is important that, if upwind differencing is used for ϕ_η, it should also be used for z_η; similar remarks hold for ϕ_ζ and z_ζ. It is now clear that upwind differences may be needed to represent the first-order derivatives appearing explicitly in Eqn. (25) for the determination of R. Due to the different origin of the term J^2 in Eqn. (25), the derivatives appearing in J^2 may be represented by central-difference approximations.

d. Determination of Forcing Function Q for Boundary-Layer-Dependent Mesh System

The basic numerical transformation procedure provides a means for generating surface-oriented coordinates, with the forcing functions providing control on the spacing of the coordinates in the physical domain. However, a systematic procedure is not available for setting up the variable spacing of the coordinates or for determining the forcing function necessary to achieve that spacing. In the present work, a method has been developed to compute the forcing function $Q(\eta)$ that leads to a mesh-point distribution along a ζ=constant coordinate such that certain prescribed criteria are satisfied. The boundary layer theory is used to establish an important one of these criteria; hence, the resulting mesh system is referred to as a boundary-layer dependent coordinate system.

The discussion presented here is with reference to flow past an airfoil. However, the concept is general and can be easily adapted to other flow problems. Based on experimentation with an inviscid subsonic flow solution for an airfoil at incidence of up to 30° and an analysis of truncation errors of the finite-difference transformation equations, the desired spacing of the η-coordinates is required to satisfy the following criteria:

a. A minimum number K of η-lines must be placed in the boundary layer on the airfoil surface.

b. The maximum step size $(\Delta\phi)_{max}$ adjacent to the far-field boundary should be approximately unity (in non-dimensional variables) except when this boundary is placed at infinity.

c. The grid spacing in the boundary layer should correspond to constant increments in the flow variable with the largest normal gradient.

d. Second-order derivatives of the mesh spacing must be minimized.

The first two criteria serve to provide appropriate resolution of the boundary-layer region near the airfoil as well as the far-field region of the flow field. Presently, the flow in the boundary-layer region is being represented by the Blasius series, for the purpose of the mesh generation. Although a more accurate representation of this flow is easily obtainable, the simple Blasius solution was used in developing this procedure. The far-field boundary is located at approximately ten chord-lengths from the airfoil surface and is circular in shape; a more appropriate shape for the outer boundary is described later in this report. A total of 44 points is used along the η-direction.

The last two criteria are used to minimize the truncation errors in the finite-difference solution. Difference approximations for the Navier-Stokes equations are usually second-order accurate in the transformed coordinates. Therefore, the truncation error in these approximations is proportional to third- and higher-order derivatives of the flow variables. In the boundary-layer region, normal gradients of the streamwise velocity w are larger than most other gradients. Therefore, if the consecutive η-coordinates are placed at constant increments of w, as suggested by Thompson[4], then

$$\frac{\partial w}{\partial \eta} = \text{constant}$$

and

$$\frac{\partial^2 w}{\partial \eta^2} = \frac{\partial^3 w}{\partial \eta^3} = \ldots = 0 \quad .$$

Furthermore, if the same w-increment is employed for the η-lines at each streamwise location, then

$$\frac{\partial w}{\partial \zeta} = \frac{\partial^2 w}{\partial \zeta^2} = \frac{\partial^3 w}{\partial \zeta^3} = \ldots = 0 \quad .$$

The spacing of the η-coordinates within the boundary-layer can thus be determined from the velocity profiles for a boundary-layer solution, such that the truncation error is minimized. Since the analysis essentially optimizes the η-line spacing with respect to the gradient of one variable in one direction, the validity of the analysis depends on the validity of the boundary-layer approximation for the problem under consideration.

The need for minimizing the second-order derivatives of the coordinates is explained as follows. For a simple stretching transformation in the physical plane, the truncation error associated with a central-difference approximation for a first-order derivative is obtained as

$$w_\phi = [w_\eta/\phi_\eta]_c - \frac{\Delta\eta}{2} [\phi_{\eta\eta}]_c w_{\phi\phi} + \ldots$$

where c denotes central difference. Therefore, the truncation error introduces an artificial-viscosity term proportional to $\phi_{\eta\eta}$, so that $\phi_{\eta\eta}$ must be minimized. Moreover, the transformation of the second-order derivative as

$$w_{\phi\phi} = \phi_\eta^2 w_{\eta\eta} + \phi_{\eta\eta} w_\eta \quad ,$$

together with central-difference representations for w_η and $w_{\eta\eta}$, shows that $\phi_{\eta\eta}$ has an adverse influence on the diagonal dominance of the finite-difference equations. This, again, indicates that $\phi_{\eta\eta}$ must be minimized.

All of the above criteria must be satisfied simultaneously. Also, for maximum usefulness, the procedure must be as automated and as simple as possible. Approximating the body surface locally as a flat plate, the transformation equation for the normal coordinate is given by Eqn. (9). With a forcing function of the form

$$Q = -A\, e^{-D\eta} \quad , \tag{31}$$

Eqn. (9) can be integrated once to yield

$$\left(\frac{d\eta}{d\phi}\right)^2 = 2\ \frac{A}{D}\ e^{-D\eta} \quad . \tag{32}$$

Here, the constant of integration has been set to zero by assuming that $\partial\eta/\partial\phi \to 0$ as $\phi \to \phi_\infty$. Evaluating Eqn. (32) at the body surface $\eta = 0$ yields an estimate for A/D, in terms of the step size $\Delta\phi_{min}$ required near the body surface, as

$$\frac{A}{D} = \frac{1}{2}\ (\Delta\eta/\Delta\phi_{min})^2 \quad . \tag{33}$$

Evaluating Eqn. (32) at $\eta = (\eta_{max} - \frac{\Delta\eta}{2})$ yields an estimate for D, in terms of the step size $\Delta\phi_{max}$ near the outer boundary, as

$$D = \ell n[2\ \frac{A}{D}\ (\frac{\Delta\eta}{\Delta\phi_{max}})^2]/[\eta_{max} - \frac{\Delta\eta}{2}] \quad . \tag{34}$$

To place K points within the boundary layer, the forcing function used is

$$Q = -\sum_{k=1}^{K} A_k\, e^{-D|\eta-\eta_k|} \tag{35}$$

where $\eta_k = (k-1)\Delta\eta$. With this Q, integration of Eqn. (9) leads to

$$\left(\frac{d\eta}{d\phi}\right)^2 = \sum_{k=1}^{K} 2\,\frac{A_k}{D}\left\{e^{-D\mu(\eta,\eta_k)} + [\mathrm{sgn}(\eta_k-\eta),0]\left[1-e^{-D|\eta-\eta_k|}\right]\right\} \tag{36}$$

where

$$\mu(\eta,\eta_k) = \begin{cases} 0 & \text{for} \quad \eta \le \eta_k \ ; \\ \eta-\eta_k & \text{for} \quad \eta > \eta_k \ ; \end{cases}$$

$$\mathrm{sgn}(\eta_k-\eta) = \begin{cases} +1 & \text{for} \quad \eta_k-\eta \ge 0 ; \\ -1 & \text{for} \quad \eta_k-\eta < 0 . \end{cases}$$

Evaluating Eqn. (36) at $\eta_i = (i+1/2)\Delta\eta$ for $i = 1, 2, \ldots, (K-1)$, leads to (K-1) simultaneous equations for A_k/D for $k = 1, 2, \ldots, K$, with D determined from a modification of Eqn. (34) as

$$D = f\ \ell n\left[2\,\frac{A}{D}\left(\frac{\Delta\eta}{\Delta\phi_{max}}\right)^2\right]/\left(\eta_{max} - \frac{\Delta\eta}{2} - K\right) \tag{37}$$

where f is a weighting factor, = 1.1. The system of equations for A_k/D is completed by a constraint relating Eqns. (32) and (36) so that

$$\sum_{k=1}^{K} A_k = g\,A \tag{38}$$

where g is a constant, = 0.4.

The (K-1) values of $\Delta\phi_i$ required in Eqn. (36) are determined, so as to minimize $\partial w/\partial\eta$, using a Newton-Raphson iteration with the Blasius series solution for the velocity $F(\tilde{\eta})$ in a flat-plate boundary layer. Here, $\tilde{\eta}$ is the boundary-layer ordinate, determined

iteratively by the relation

$$\tilde{\eta}_i^{(s+1)} = \tilde{\eta}_i^{(s)} - (F_i - 2w_i)/(F_i' + 0.01) \qquad (39)$$

where $i = 1, 2, \ldots, K$,

$$F_i = a\,\tilde{\eta}_i - \frac{a^2}{4!}\,\tilde{\eta}_i^4 + \frac{11a^3}{7!}\,\tilde{\eta}_i^7 - \frac{375a^4}{10!}\,\tilde{\eta}_i^{10} \quad ,$$

$$a = 1.32824 \quad , \quad F' = \partial F/\partial\tilde{\eta} \quad , \quad w_i = i/(K+1) \quad ,$$

and s denotes iteration number.

The physical ordinate is then given as

$$\phi_{i,B} = 2\tilde{\eta}_i \sqrt{z/(W_e Re)} \qquad (40)$$

where W_e is the velocity at the edge of the boundary layer. If, instead of prescribing K, it is desired to specify the constant increment Δw, then the corresponding value of K is determined, by integer arithmetic, using the relation

$$K = (W_e/\Delta w - 0.01). \qquad (41)$$

The procedure described above was employed to generate the forcing function, Q, for various values of the parameters for a test case. The corresponding ϕ-distribution is then determined by numerical solution of Eqn. (9). The second-order derivative $\phi_{\eta\eta}$ was approximated by a central difference, while upwind differencing was used for the unknown ϕ_η. A quasilinearized tridiagonal scheme of solution required about 20 iterations, whereas a linearized successive over-relaxation (SOR) scheme with optimized acceleration parameters required about 40 iterations. Figure 6 shows the results obtained for Q, ϕ, ϕ_η and $\phi_{\eta\eta}$ for z = 1.0,

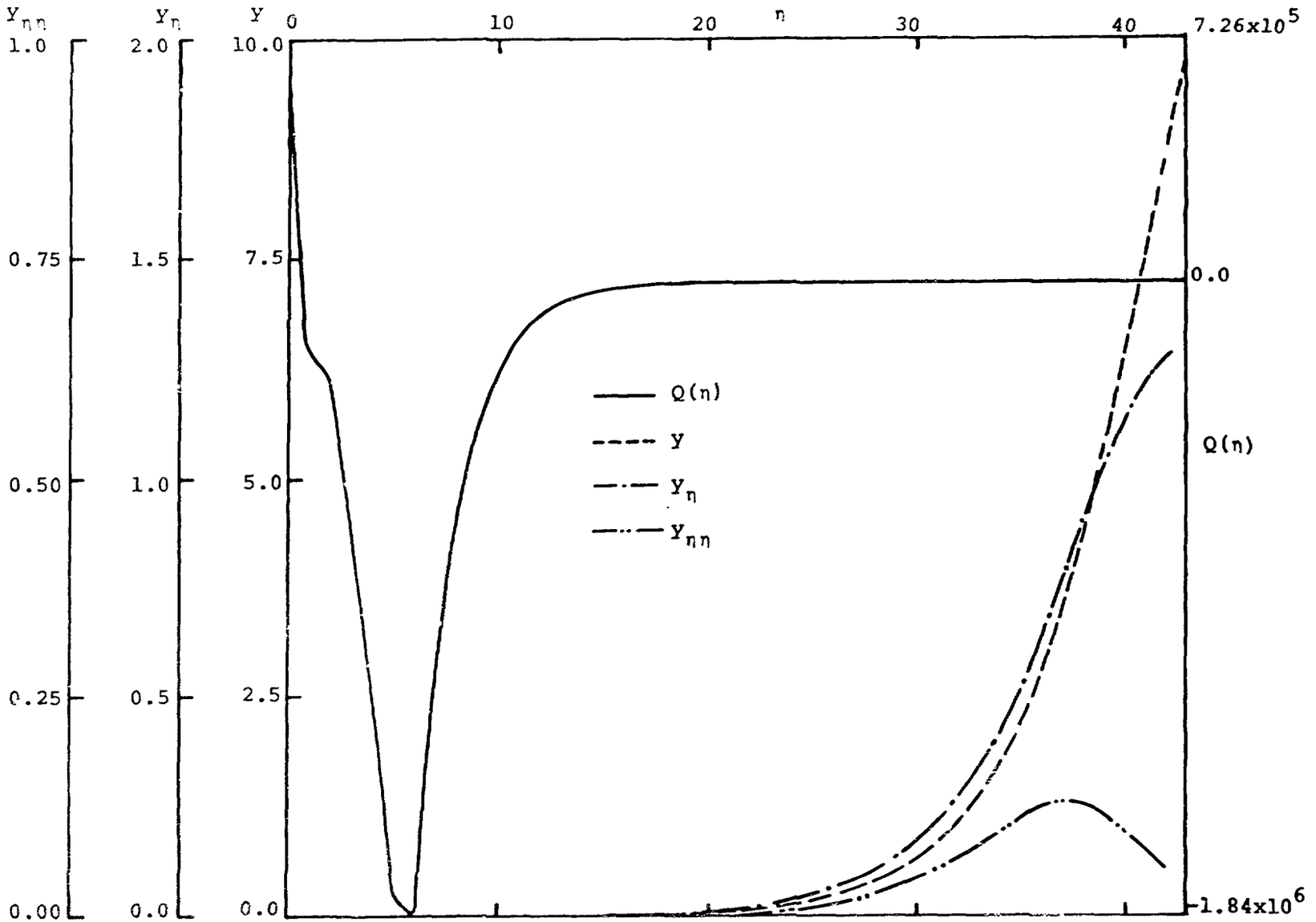

FIG. 6. FORCING FUNCTION AND COORDINATE DERIVATIVES FOR BOUNDARY-LAYER DEPENDENT MESH FOR NACA0018 AIRFOIL, Re = 2 x 10^6, z = 1.0.

$Re = 2 \times 10^6$, $\eta_{max} = 43$, $\Delta\eta = 1$, and $W_e = 1.2$, $\Delta w = 0.15$ so that $K = 7$. The computed values of ϕ_i are compared with the desired values of ϕ_i in Table I which also lists the corresponding values of Q_i. It is seen that the procedure leads to a very satisfactory mesh-point distribution.

The procedure has also been applied at various streamwise locations, downstream of 5 percent chord, on a NACA 0018 airfoil. For simplicity, a Blasius profile, with a constant velocity at the edge of the boundary layer, has been used. The first 20 η-lines in a (71 x 44) boundary-layer-dependent mesh system are shown in Fig. 7 for $Re = 2 \times 10^6$, $\eta_{max} = 43$, $\Delta\eta = 1$, $W_e = 1.2$, $\Delta w = 0.15$, with $K = 7$.

Some improvements can be made in this automated procedure, for example, by using the appropriate inviscid velocity W_e and then specifying the correct boundary-layer profile from a boundary-layer solution. However, the improvement would be limited by the extent of validity of the boundary-layer solution. Therefore, difficulty may be encountered in regions of large surface-curvature where the transformed coordinate ζ=constant may not be orthogonal to the body surface.

TABLE I

SOLUTION OF $\phi_{\eta\eta} + Q\phi_{\eta}^{3} = 0$ WITH BLASIUS BOUNDARY-LAYER DEPENDENT Q(η) FOR NACA 0018 AIRFOIL AT Re = 2×10^{6}, z = 1.0

η_i	$Q_i \times 10^{-6}$	$\phi_{i,\text{Blasius}}$	$\phi_{i,\text{computed}}$
0	0.72603	0.000243	0.000248
1	-0.19147	0.000487	0.000500
2	-0.27910	0.000736	0.000756
3	-0.67778	0.000996	0.001024
4	-1.1501	0.001280	0.001316
5	-1.7853	0.001610	0.001660
6	-1.8412	0.002077	0.002103
7	-1.1115		0.002672
8	-0.67517		0.003402
9	-0.40885		0.004342
10	-0.24758		0.005548
11	-0.14993		0.007099
12	-0.09079		0.009092
13	-0.05498		0.011653
14	-0.03329		0.014945
15	-0.02016		0.019174
16	-0.01221		0.024609
17	-0.00739		0.031593
18	-0.00448		0.040568
19	-0.00271		0.052100

TABLE I (continued)

η_i	$Q_i \times 10^{-6}$	$\phi_{i,Blasius}$	$\phi_{i,computed}$
20	-0.00164		0.066920
21	-0.00099		0.085963
22	-0.00060		0.11043
23	-0.00036		0.14187
24	-0.00022		0.18226
25	-0.00013		0.23414
26	-0.00008		0.30076
27	-0.00005		0.38628
28	-0.00003		0.49600
29	-0.00002		0.63660
30	-0.00001		0.81651
31	-0.00000		1.0461
32	-0.00000		1.3381
33	-0.00000		1.7072
34	-0.00000		2.1696
35	-0.00000		2.7416
36	-0.00000		3.4370
37	-0.00000		4.2631
38	-0.00000		5.2183
39	-0.00000		6.2904
40	-0.00000		7.4596
41	-0.00000		8.7033
42	-0.00000		10.0000

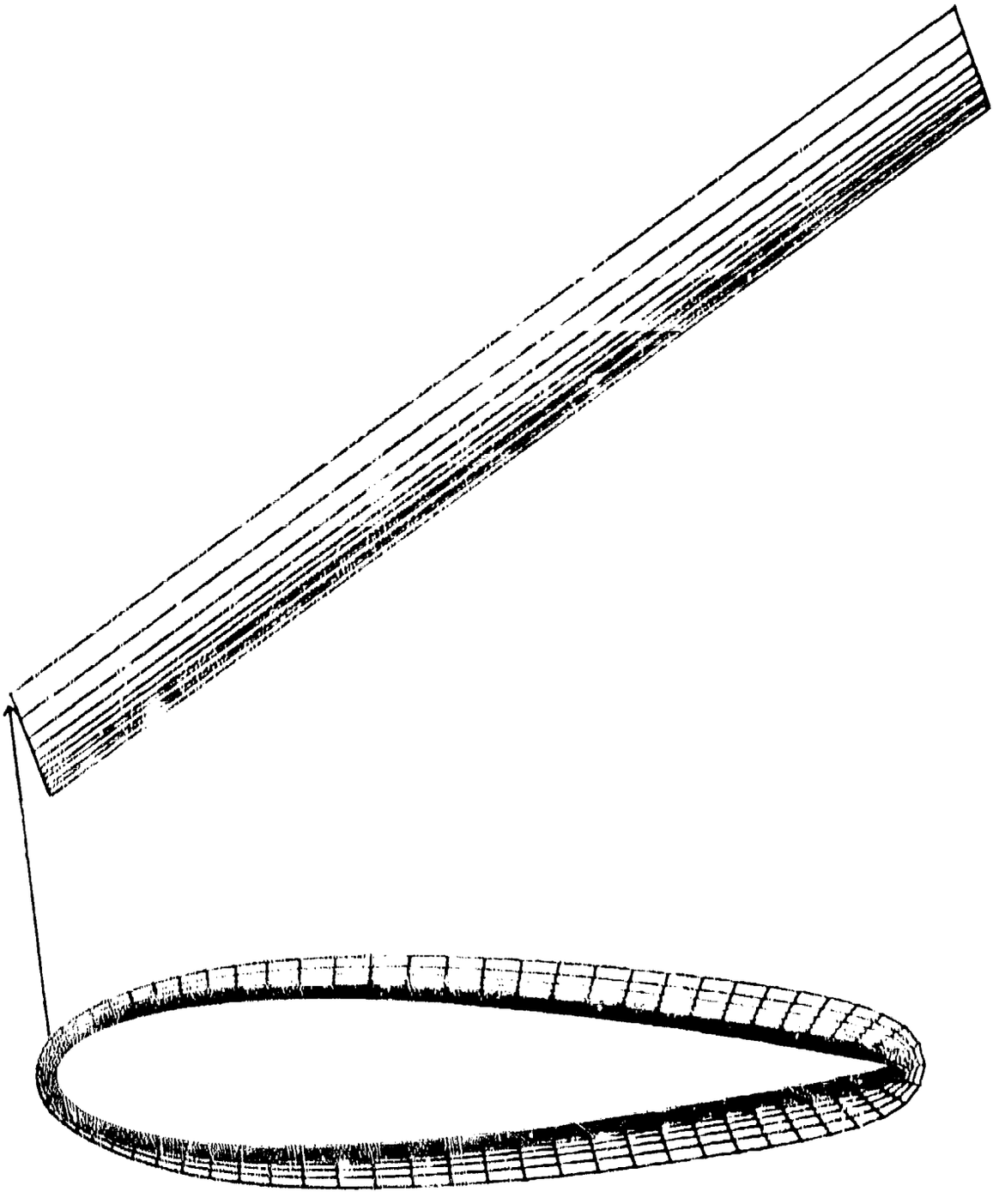

FIG. 7, BOUNDARY-LAYER-DEPENDENT MESH SYSTEM FOR NACA0018 AIRFOIL. $Re = 2 \times 10^6$.

2. LOCATION OF FAR-FIELD BOUNDARY FOR SUBSONIC EXTERNAL FLOW

a. Far-Field Boundary at Infinity

A major question that arises in the study of subsonic flow past a body concerns the shape and location of the far-field boundary for the solution domain. From the viewpoint of analytical rigor, this boundary is ideally located infinitely far from the body. The unbounded physical domain must then be mapped to a finite domain by an appropriate analytical transformation based on the asymptotic behavior of the flow far from the body. The analytical transformation can also serve to provide, at least partially, the stretching of some of the critical regions in the flow field. The resulting coordinates can be made to be surface-oriented along all boundaries except along the surface of the arbitrary body. These coordinates are then transformed numerically to achieve complete surface-orientation and the final desired stretching of the various regions of the problem domain. This combination of analytical and numerical transformations also considerably relieves the burden of the numerical transformation.

As regards the shape of the far-field boundary, it appears that, for a large class of two-dimensional or axisymmetric flows past finite bodies, a parabolic shape may be suitable for an outer boundary. This configuration permits one of the transformed coordinates to be oriented along the same general direction as the main flow, so that the associated numerical solution can have better convergence properties. Therefore, it may be more appropriate to set up the numerical transformation in terms of parabolic coordinates rather than Cartesian or cylindrical coordinates,

after mapping them to a finite domain. Thus, the total transformation procedure would consist of the following steps:

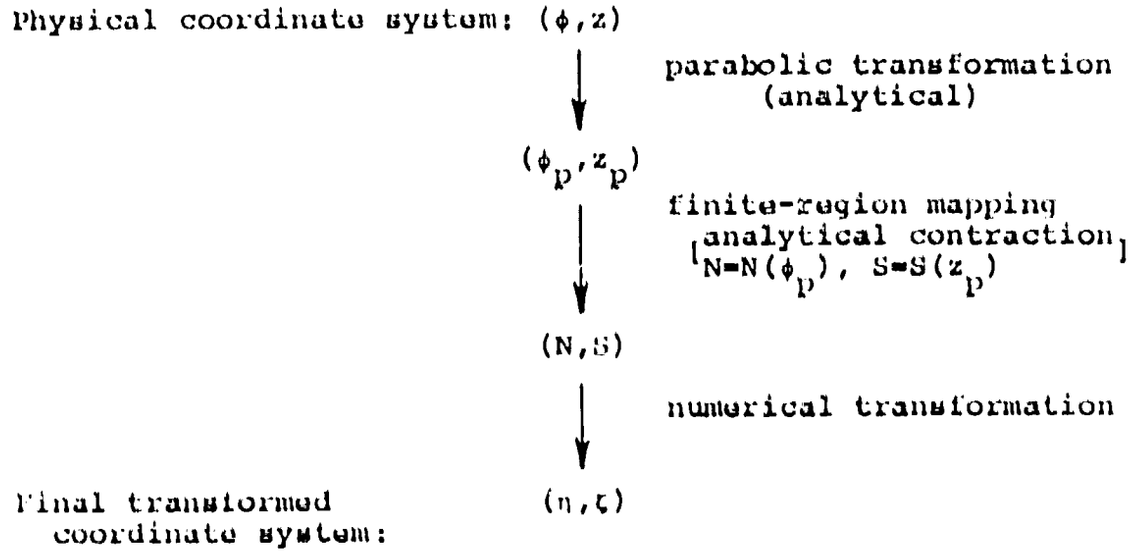

Two approaches present themselves at this stage, regarding the equations to be used to accomplish the numerical transformation. In the equations used so far, the elliptic operator employed has been the Laplacian operator. In order to conform to this, it would now be necessary to formulate the Laplacian operator in terms of the (N,S) coordinates as independent variables. The corresponding Poisson equations for the coordinates η, ζ then need to be inverted to make η, ζ the independent variables and N, S the dependent variables. Therefore, in this approach, the numerical transformation would employ the true Laplacian, so that the equations to be inverted are

$$\nabla^2_{N,S}\eta = Q \qquad \text{and} \qquad \nabla^2_{N,S} = R \tag{42a,b}$$

where $\nabla^2_{N,S}$ is the Laplacian in (N,S) coordinates and is obtained as

$$\nabla^2_{N,S} = \frac{1}{h^2}\left[(N')^2 \frac{\partial^2}{\partial N^2} + N'' \frac{\partial}{\partial N} + (S')^2 \frac{\partial^2}{\partial S^2} + S'' \frac{\partial}{\partial S}\right] \quad (43)$$

with primes denoting differentiation of a variable with respect to its argument. Also, h is the scale factor for the parabolic transformation

$$z + i\phi = \frac{1}{2}(z_p + i\phi_p)^2 \quad , \quad (44)$$

so that

$$h^2 = \phi_p^2 + z_p^2 \quad . \quad (45)$$

The inversion of Eqs. (42a,b) leads to the following equations for the numerically transformed coordinates:

$$\bar{a}\, N_{\eta\eta} + 2\bar{b}\, N_{\eta\zeta} + \bar{c}\, N_{\zeta\zeta} - N'' + h^2 \bar{J}^2 (QN_\eta + RN_\zeta) = 0$$

$$\bar{a}\, S_{\eta\eta} + 2\bar{b}\, S_{\eta\zeta} + \bar{c}\, S_{\zeta\zeta} - S'' + h^2 \bar{J}^2 (QS_\eta + RS_\zeta) = 0 \quad (46a,b)$$

where

$$\bar{a} = N_\zeta^2 S'^2 + S_\zeta^2 N'^2 \quad ,$$

$$\bar{b} = -(N_\eta N_\zeta S'^2 + S_\eta S_\zeta N'^2) \quad ,$$

$$\bar{c} = N_\eta^2 S'^2 + S_\eta^2 N'^2 \quad ,$$

$$\bar{J} = N_\eta S_\zeta - N_\zeta S_\eta \quad . \quad (47)$$

It should be noted that h^2 as well as the quantities N', N'', S', S'' must be expressed in terms of N and S in the above equations. The details of the derivation of Eqs. (46a,b) are described in Appendix B.

In an alternate approach, it seems that, for the coordinate equations, perhaps it is not essential to work with a true Laplacian operator. Another elliptic operator that satisfies the maximum principle would also be satisfactory. Of course, the choice of the Laplacian was guided by its similarity to the equations for the corresponding inviscid-flow stream function and potential function. For reasons of mathematical simplicity, the following system of equations for the numerically transformed coordinates may be preferable:

$$\eta_{NN} + \eta_{SS} = Q \; ; \qquad \zeta_{NN} + \zeta_{SS} = R \quad . \tag{48a,b}$$

The corresponding inverted equations for the N,S coordinates are of the same form as Eqs. (4-7).

Boundary conditions specified in the (ϕ,z) domain must be expressed in terms of the (N,S) variables, through use of the parabolic transformation, followed by the analytical contraction transformation.

Before describing any results obtained with these combined transformation procedures, the discussion presented in the following section must be taken into consideration.

b. Far-Field Boundary at Finite Distance From Body

In many practical situations, it may not be essential to locate the far-field boundary at true infinity. For example, analyses of flow over a cylinder have frequently employed a far-field boundary located at about 10 cylinder-radii from the cylinder[9]. As shown below, this is the location where the free-stream pressure is disturbed by less than one percent due to the presence of the cylinder in the flow. For incompressible inviscid flow past a cylinder of radius r_o, the pressure coefficient C_p is expressed as

$$C_p = \frac{p - p_\infty}{\rho U_\infty^2} = \frac{1}{2}\left(1 - \frac{V^2}{U_\infty^2}\right) \tag{49}$$

where the subscript ∞ denotes free-stream conditions. Here, V is the local total velocity in the flow given as follows, in terms of the radial and tangential velocity components u_r and u_θ, respectively,

$$V^2 = u_r^2 + u_\theta^2 \tag{50}$$

where

$$u_r = U_\infty\left(1 - \frac{r_o^2}{r^2}\right)\cos\theta \quad ,$$

$$u_\theta = -U_\infty\left(1 + \frac{r_o^2}{r^2}\right)\sin\theta \quad . \tag{51}$$

Substituting Eqs. (50-51) in Eq. (49) gives, after simplification,

$$C_p = \frac{\cos 2\theta}{(r/r_o)^2} - \frac{1}{2(r/r_o)^4} \quad . \tag{52}$$

This implies that

$$|C_p|_{max} = 0.01 \quad \text{when} \quad r/r_o \simeq 10 \; . \tag{53}$$

Therefore, an appropriate far-field boundary for the flow past a cylinder would encompass at least the region shown in the following sketch.

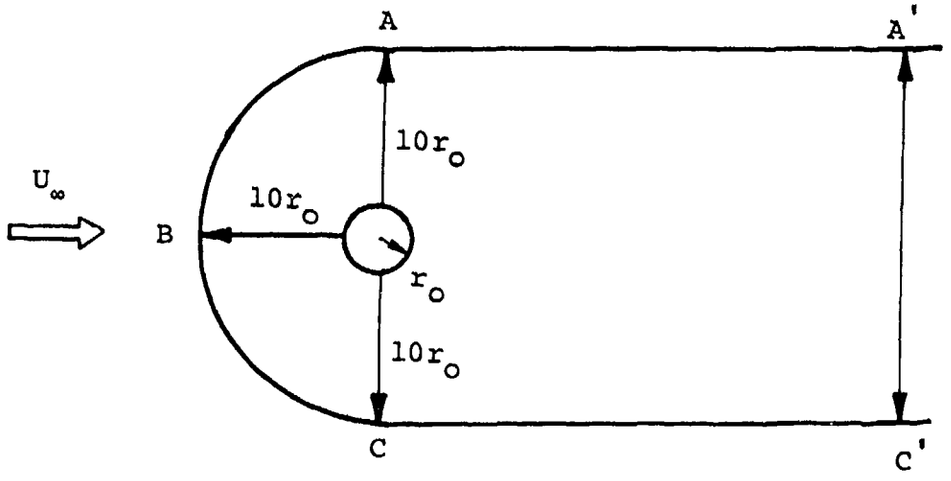

FIG. 8. LOCATION OF FAR-FIELD BOUNDARY FOR FLOW PAST A CIRCULAR CYLINDER.

For viscous flow calculations, it would be more desirable to have a far-field boundary such that the distance A'C' increases approximately as the square-root of the streamwise distance.

The above analysis can also be employed to estimate the extent of the region in which the inviscid pressure for flow past an airfoil is disturbed by less than one percent. A symmetric Joukowski airfoil is considered here for this purpose. With a Joukowski transformation, a cylinder of radius $(r_o + \alpha)$, with center at $(-\alpha, 0)$, transforms to a Joukowski airfoil of chord $\ell \simeq 4r_o(1+\varepsilon^2)$ and thickness ratio $t_{max}/\ell \simeq (3\sqrt{3}/4)\varepsilon$, where ε is the eccentricity defined as $\varepsilon = \alpha/r_o$. Since the inviscid flow past the airfoil is obtainable by transformation of the flow past a cylinder, the region of disturbed inviscid flow for the airfoil is also obtainable by transformation of the region of disturbed inviscid flow for the cylinder. Accordingly, it is necessary to

transform a larger circle of radius $(10r_o + 10\alpha)$ with center at $(-10\alpha, 0)$ using the Joukowski transformation. This results in a larger Joukowski airfoil of chord $L \simeq 40\ r_o(1 + \varepsilon^2)$ and maximum thickness $T_{max} \simeq 30\sqrt{3}\ \alpha$. The eccentricity and the thickness ratio of the larger airfoil are the same as those for the original airfoil. With reference to the chord of the original airfoil, the boundary of the region of disturbed inviscid flow past the airfoil is obtained as a large Joukowski airfoil of

$$\text{chord} \qquad L/\ell = 10 \quad ,$$

$$\text{maximum thickness} \qquad T_{max}/\ell \simeq \frac{15}{2}\sqrt{3}\,\varepsilon = 13\varepsilon \quad . \tag{54}$$

Therefore, for a 10-percent thick airfoil at zero incidence, a far-field boundary based on the region of 1-percent inviscid-pressure disturbance would appear as shown in the following sketch.

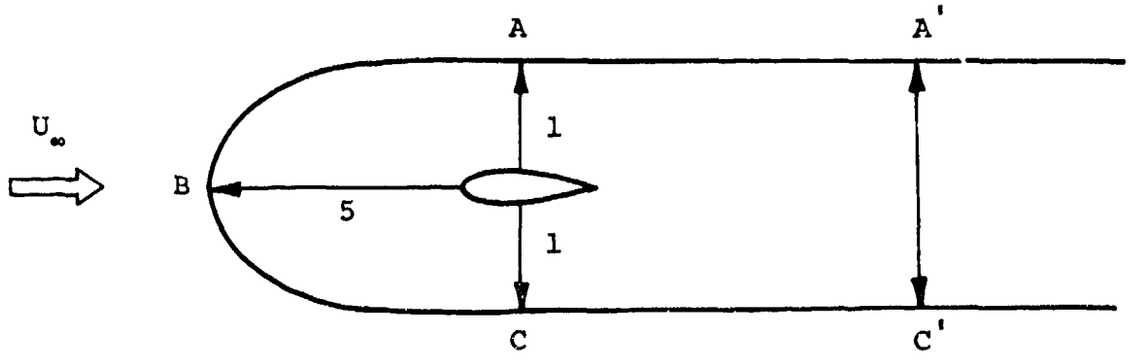

FIG. 9. LOCATION OF FAR-FIELD BOUNDARY FOR SYMMETRIC FLOW PAST A JOUKOWSKI AIRFOIL.

Again, for viscous-flow calculations, it would be desirable to have the dimension A'C' increasing with streamwise distance. For an airfoil at angle of incidence β, T_{max}/ℓ should be incremented

by (10 sinβ) to account for the increase in effective frontal area of the airfoil.

It is necessary to observe that the above analysis only provides the location of the contour of $|C_p|_{inviscid} = 0.01$. This serves as a useful guideline for the location of the far-field boundary. However, by employing the undisturbed free-stream conditions at the location of 1-percent disturbance, the error introduced in the results at the body surface may exceed 1 percent.

A study was made to assess the inferences of this analysis by computing the inviscid flow past a symmetric Joukowski airfoil of approximately 9-percent thickness ratio (i.e., $t_{max}/\ell = 0.09$), at various angles of incidence. The outer boundary for these calculations was an ellipse of major axis $2z_\infty$ and minor axis $2\phi_\infty$, with the major axis aligned with the free-stream direction. The results of these calculations are summarized in Table II. Comparison is made of the coefficients of minimum pressure $C_{p(min)}$, drag C_D, lift C_L and moment about the leading edge $C_{M(LE)}$, for various values of z_∞ and ϕ_∞. For each value of β studied, the last row corresponds to the values of z_∞ and ϕ_∞ obtained on the basis of the above analysis. It is seen that, with the far-field boundary located in accordance with the prediction of the foregoing analysis, the maximum error in C_L and $C_{M(LE)}$ is about 1 percent. The maximum error in C_D is about 0.02. However, the maximum error in $C_{p(min)}$ is almost 2.7 percent and occurs for $\beta = 10°$ and 30°. But it should be noted that, when $C_{p(min)}$ has this large error for the smallest z_∞, ϕ_∞ investigated, a major part of this error has been already incurred at the largest z_∞, ϕ_∞ investigated.

TABLE II

EFFECT OF OUTER-BOUNDARY LOCATION ON SURFACE COEFFICIENTS FOR INVISCID FLOW PAST A SYMMETRIC JOUKOWSKI AIRFOIL

β	z_∞/C	ϕ_∞/C	$C_{p,min}$	C_D	C_L	$C_{M,LE}$
	∞	∞	-0.34513	0.0	0.0	0.0
	20	20	-0.34610	-0.205×10^{-3}	-0.820×10^{-5}	-0.05×10^{-5}
0°	10	10	-0.34616	-0.196×10^{-3}	-0.083×10^{-5}	$+0.21 \times 10^{-5}$
	10	6	-0.34640	-0.189×10^{-3}	-0.069×10^{-5}	$+0.16 \times 10^{-5}$
	10	4	-0.34700	-0.179×10^{-3}	-0.290×10^{-5}	-0.05×10^{-5}
	5	2	-0.35060	-0.159×10^{-3}	-0.163×10^{-5}	-0.22×10^{-5}
	∞	∞	-9.2250	0.0	1.1667	$\approx$0.2917
	20	20	-9.4196	-0.0028	1.1700	0.2922
10°	10	10	-9.4190	-0.0027	1.1708	0.2924
	10	6	-9.4200	-0.0024	1.1727	0.2932
	10	4	-9.4390	-0.0022	1.1770	0.2949
	5	4	-9.4750	-0.0029	1.1780	0.2948
	∞	∞	-75.550	0.0	3.3593	$\approx$0.8398
30°	20	20	-77.606	-0.0186	3.3790	0.8448
	10	10	-77.594	-0.0187	3.3800	0.8451

This indicates that, at least from inviscid-flow considerations, the far-field boundary may enclose a considerably smaller region than employed so far ($z_\infty = \phi_\infty = 10$ for $\beta = 0$), without significantly affecting the accuracy of the results. The conclusion arrived at in Ref. 9 for the proper values of z_∞, ϕ_∞ must be because of the considerably larger values computed there for ΔC_D and ΔC_L for $\beta = 0$.* With the general procedure very similar to that in Ref. 9, the present results show much smaller ΔC_D and ΔC_L. A closer examination reveals a difference in the manner C_p is integrated along the body surface, to compute C_D and C_L. Considering the trapezoidal rule, the integral of C_p around the body contour was represented in Ref. 9 as

$$\oint C_p \, ds = \oint C_p \, g \, d\xi = \sum_{i=2}^{IMAX} [f_i + f_{i-1}] \frac{\Delta\xi}{2} \qquad (55)$$

where $f_i = C_{p_i} g_i$ and g consists of the scale facotrs of the transformation evaluated at the body surface s. However, since g enters this integral through the relation $ds = g \, d\xi$, it has been found more appropriate to represent the integral in the following form:

$$\oint C_p \, ds = \sum_{i=2}^{IMAX} \frac{1}{2} [C_{p_i} + C_{p_{i-1}}][g_i + g_{i-1}] \frac{\Delta\xi}{2} \qquad (56)$$

Experience with other problems[10] has also indicated that the product of terms in integrands be represented as the product of the average values of the terms, rather than as the average of the product.

---

* Here, the prefix Δ denotes deviation from the theoretical values.

3. ORTHOGONALIZATION OF COORDINATES

As mentioned in the Introduction, it is frequently desirable to work with an orthogonal or near-orthogonal coordinate system. Non-orthogonality leads to a non-zero coefficient of the mixed-derivative terms in the coordinate equations as well as in the flow equations. Most numerical schemes available, even implicit ones, treat mixed derivatives in an explicit manner. This tends to retard the convergence rate of the numerical solution. Mitchell[11] has discussed a second-order accurate finite-difference representation for treatment of the mixed derivative. The representation takes different forms depending on the relative values of the coefficients a, b, c in the governing equations (4-5). The further analysis of Greenspan and Jain[12] relaxed some of the conditions obtained by Mitchell. However, implementing these representations in the implicit alternating-direction numerical scheme presently employed did not lead to a gain in computational efficiency. It is possible that this implementation of the mixed derivative was still not fully implicit; further work is indicated in this area. These considerations do not arise in the case of nearly orthogonal coordinates, when the mixed-derivative terms have coefficients that are nearly zero.

An effort is made in the present work to develop a procedure for obtaining a system of orthogonal or near-orthogonal coordinates, starting with a given non-orthogonal coordinate system. The starting system is determined as the solution of the coordinate equations (4-7) using the appropriate forcing

function Q for the end boundaries, with consistent distribution of the points along these boundaries. The forcing function R must be consistent with the desired distribution of points on the lower and the upper boundaries. Also, the boundary coordinates must be orthogonal at the corners.

This solution generally yields a good set of body-oriented coordinates. However, the coordinate-system will not necessarily be orthogonal because the distribution of points on the far-field boundary may not be consistent, as regard orthogonality, with the point distribution on the lower boundary containing the body surface. Therefore, the coordinates must be adjusted so as to produce an orthogonal system. For this purpose, the streamwise coordinates, i.e., the curves of η=constant, are retained. The ζ-coordinates are altered so as to satisfy the condition of local orthogonality, Eq. (20), i.e.

$$\phi_\eta \, \phi_\zeta + z_\eta \, z_\zeta = 0 \quad . \tag{20}$$

Starting at the lower boundary, the ζ-curves are altered in a step-by-step manner, over each $\Delta\eta$ step, as illustrated below.

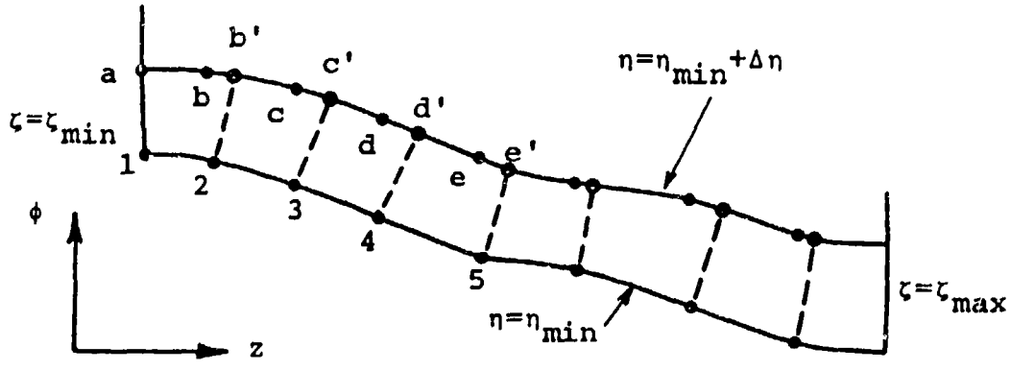

FIG. 10. STEP-BY-STEP ORTHOGONALIZATION.

The above sketch shows two coordinate curves $\eta = \eta_1$ and $\eta = \eta_1 + \Delta\eta$, with dots denoting the starting position of the points obtained from the solution of the coordinate equations. It is required to determine the positions of points such as b', c', d', etc., such that the resulting coordinate system is orthogonal. To locate b', for example, ϕ_ζ and z_ζ are computed as the average of their values at points '2' and b, using the non-orthogonal solution along η_1 and $(\eta_1+\Delta\eta)$. Thus,

$$\phi_\zeta\Big|_{2b} = \frac{1}{2}\left[\frac{(\phi_3-\phi_1)+(\phi_c-\phi_a)}{2\Delta\zeta}\right]$$

and

$$z_\zeta\Big|_{2b} = \frac{1}{2}\left[\frac{(z_3-z_1)+(z_c-z_a)}{2\Delta\zeta}\right] \quad . \tag{57}$$

Next, ϕ_η and z_η are computed from the known non-orthogonal solution as

$$\phi_\eta\Big|_{2b} = \frac{\phi_b-\phi_2}{\Delta\eta} \quad , \quad z_\eta\Big|_{2b} = \frac{z_b-z_2}{\Delta\eta} \quad . \tag{58}$$

Then, the left-hand side of the condition of orthogonality, Eq. (20), is evaluated to yield δ_{2b} as

$$\delta_{2b} = \frac{z_\eta}{\phi_\eta}\Big|_{2b} + \frac{\phi_\zeta}{z_\zeta}\Big|_{2b} \quad . \tag{59}$$

If $\delta_{2b} \neq 0$, the calculation proceeds to the next point along the $(\eta_1+\Delta\eta)$-curve, to evaluate δ_{2c}, δ_{2d}, etc., until a change in sign is encountered by the left-hand side of Eq. (20). For the sketch shown, this would occur between b and c for point '2'. Then, b'

is located between b and c, using linear interpolation, yielding $\delta_{2b'} = 0$ and, hence, a locally orthogonal coordinate system in the vicinity of point '2'.

The procedure is repeated for point '3' on the η_1-curve, beginning with point b on the $(\eta_1+\Delta\eta)$ curve and, similarly, for all points up to $(\zeta_{max}-\Delta\zeta)$ on the η_1-curve. The procedure is then repeated for the pair of η-coordinates given by $(\eta_1+\Delta\eta)$= constant and $(\eta_1+2\Delta\eta)$=constant, using the points b', c', d', etc., on the $(\eta_1+\Delta\eta)$-curve. Continuing successively for all the η-coordinates until the upper boundary $\eta=\eta_{max}$ is encountered, this will result in a coordinate system that is locally orthogonal at all the grid points. It is to be noted that only two-dimensional configurations can be considered by this approach, at present.

The procedure performs best when the η-coordinates have only convex curvature or minimal concave curvature and, in these cases, no restriction is required on the degree of non-orthogonality of the starting coordinate system. However, when the η-coordinates contain regions of large concave curvature, the procedure may lead to cross-over of the new ζ-coordinates unless the local mesh aspect ratio $(\Delta z/\Delta\phi)$ in the physical plane equals or exceeds unity. This requirement may be related to the Cauchy-Riemann conditions which are more restrictive than the condition of orthogonality [see Appendix A].

a. Partial Orthogonalization

Situations may arise where the surface coordinate $\eta = \eta_1$ may contain a point of discontinuous slope, e.g., near the trailing edge of an airfoil. For these configurations, it is desirable to require the altered coordinate system to be orthogonal everywhere except in the vicinity of the point of discontinuous slope. In this vicinity, the coordinate curves are required to intersect at a specified angle related to the angle in the surface coordinate at this point. This may be achieved by a procedure described below.

The following sketch shows a portion of the surface coordinate $\eta = \eta_1$ which has a discontinuity at point C. This discontinuity may be represented by the angle γ, which differs from π.

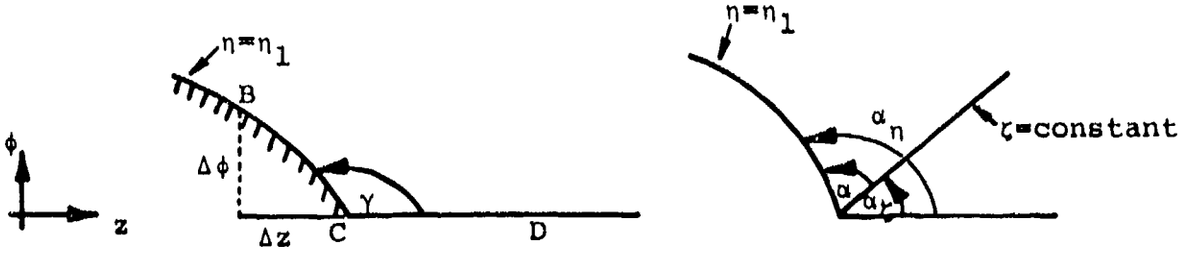

FIG. 11. ANGLE BETWEEN COORDINATE CURVES.

In terms of surface points immediately adjacent to point C,

$$\gamma = \pi - \tan^{-1} |\Delta\phi/\Delta z| \quad . \tag{60}$$

For partial orthogonalization near the point C, the angle between the η-coordinate line through C and the η_1-coordinate should

be $\gamma/2$ on either side of the discontinuity. Now, the angle of intersection between the η- and ζ-coordinates can be obtained from the relation

$$\tan\alpha = \tan(\alpha_\eta - \alpha_\zeta) = \frac{\tan\alpha_\eta - \tan\alpha_\zeta}{1 + \tan\alpha_\eta \tan\alpha_\zeta} \quad . \tag{61}$$

Noting that $\tan\alpha_\zeta = \frac{\partial\phi}{\partial z}\big|_\zeta = \phi_\eta/z_\eta$ and $\tan\alpha_\eta = \frac{\partial\phi}{\partial z}\big|_\eta = \phi_\zeta/z_\zeta$, Eq. (60) becomes

$$\tan\alpha = \frac{\phi_\zeta/z_\zeta - \phi_\eta/z_\eta}{1+(\phi_\zeta/z_\zeta)(\phi_\eta/z_\eta)}$$

$$\text{i.e.,} \qquad \tan\alpha = \frac{\phi_\zeta z_\eta - \phi_\eta z_\zeta}{z_\zeta z_\eta + \phi_\zeta \phi_\eta} \tag{62}$$

Using Eqs. (6-7), this can be expressed simply as

$$\tan\alpha = J/b \quad . \tag{63}$$

Since b is a measure of non-orthogonality of the coordinates, Eq. (63) implies that b approaches zero where the coordinates are nearly orthogonal. On the other hand, the Jacobian J is never zero or infinite for a one-to-one transformation. Therefore, it is better to work with $\cot\alpha$ expressed from Eq. (63) as

$$\cot\alpha = b/J \quad . \tag{64}$$

Therefore, the partial-orthogonalization procedure consists of defining $\alpha_{i,j}$, for each computational point (i,j) as

$$\cot\alpha_{i,j} = -[\mathrm{sgn}(j-jc)][\cot\tfrac{\gamma}{2}]\, e^{-f_{i,j}}\, e^{-|g_{i,j}|} \cos f_{i,j} \cos g_{i,j} \tag{65}$$

where

$$\mathrm{sgn}(j-jc) = \begin{cases} -1 & \text{for } (j-jc) \leq 0 \\ +1 & \text{for } (j-jc) > 0 \end{cases},$$

$$f_{i,j} = \frac{\pi}{2}\left[\frac{\phi_{i,j} - \phi_{1,jc}}{\phi_{Imax,j} - \phi_{1,jc}}\right],$$

$$g_{i,j} = \frac{\pi}{2}\left[\frac{z_{i,j} - z_{1,jc}}{z_{i,jo} - z_{1,jc}}\right],$$

with

$$j_o = \begin{cases} 1 & \text{for } j < jc \\ Jmax & \text{for } j > jc \end{cases}. \tag{66}$$

The cosine functions have been included in Eq. (65) in order to ensure complete orthogonality near the remaining three boundaries of the problem. Use of the function [sgn(j-jc)] ensures that the curves of ζ=constant are nearly parallel in the vicinity of the point c. Here, jc represents the value of j at the point c.

Hereafter, the procedure is similar to that described in the preceding section for complete orthogonalization, with Eq. (59) now being replaced by the following for partial orthogonalization:

$$\delta_{P,2b} = (\cot\alpha_{i,j})_2 - (b/J)_{2b} \tag{67}$$

where $\delta_{P,2b}$ is the error in Eq. (64) if the ζ-coordinate at point

'2' also passes through point b. In fact, Eq. (59) may be viewed as a special case of Eq. (67) when $\cot\alpha_{i,j} = 0$, so that the complete-orthogonalization procedure is a specialization of the partial-orthogonalization procedure.

Finally, it should be recognized that the complete-orthogonalization procedure outlined in the preceding section is equivalent to that of Potter and Tuttle[13] who achieve orthogonalization by solving a Neumann boundary-value problem between each two pairs of η=constant curves. It should be possible to generalize the work of Ref. 13 to include partial-orthogonalization by modifying the homogeneous Neumann boundary conditions to nonhomogeneous Neumann boundary conditions involving $\cot\alpha_{i,j}$ as defined in Eq. (65).

SECTION IV

OPTIMIZATION OF NUMERICAL METHOD OF SOLUTION

The discussion in all of section 3 was directed towards obtaining a suitable coordinate system, using as much formalism in the procedure as possible, so as not to unduly increase the overall computer time required for generating the desired mesh. For example, the use of upwind differencing in generating highly non-uniform mesh spacing, as well as the consideration of an analytical coordinate transformation simultaneously with the numerical transformation, may be also viewed as optimization of the numerical method of solution of the transformation equations. In addition, however, some measures have also been taken to

directly optimize the numerical method itself. Two such measures have been used previously and are described elsewhere[5]. These consist of the use of an implicit numerical scheme and the simultaneous solution of the coupled equations (4) and (5) for the transformation. Another important factor contributing to the efficiency of the numerical solution is the starting solution used for these nonlinear equations; this is described here.

1. INITIALIZATION PROCEDURE

Frequently, no special care is taken to formulate the starting conditions used in an iterative numerical solution procedure. This is based on the argument that initial errors decay with exponential rapidity and have no significant influence on the solution convergence. However, for complex problems with severe nonlinearities, this has been often found to be untrue. In these situations, true nonlinear instability has been observed, i.e., small initial errors decay whereas large initial errors amplify and cause the solution to become unbounded. Therefore, in these cases, the starting solution employed plays a significant role in the success of the overall solution[14]. In general, the solution of some simplified limiting form of the governing differential equations provides a good starting solution[15]. However, for the coordinate equations, even this may not be necessary. The following simple geometrical considerations lead to a suitable initial distribution for the coordinates.

If the initialization proceeds in the direction of increasing counters i and j, the increment along a coordinate at a given station can be made to have the same ratio to the total interval along that coordinate at that station as the corresponding ratio at the preceding station. This permits explicit calculation of the initial condition. Thus, with reference to the sketch shown in Fig. 12,

$$\frac{\phi_{i,j} - \phi_{i-1,j}}{\phi_{IMAX,j} - \phi_{1,j}} = \frac{\phi_{i,j-1} - \phi_{i-1,j-1}}{\phi_{IMAX,j-1} - \phi_{1,j-1}}, \quad \frac{z_{i,j} - z_{i,j-1}}{z_{i,JMAX} - z_{i,1}} = \frac{z_{i-1,j} - z_{i-1,j-1}}{z_{i-1,JMAX} - z_{i-1,1}} \tag{68a,b}$$

Similarly, it is possible to formulate analogous expressions for initial values based entirely on information at a station following the station under consideration and set up the initialization to proceed in the direction of decreasing counters i and j. Accordingly,

$$\frac{\phi_{i,j} - \phi_{i+1,j}}{\phi_{IMAX,j} - \phi_{1,j}} = \frac{\phi_{i,j+1} - \phi_{i+1,j+1}}{\phi_{IMAX,j+1} - \phi_{1,j+1}}, \quad \frac{z_{i,j} - z_{i,j+1}}{z_{i,JMAX} - z_{i,1}} = \frac{z_{i+1,j} - z_{i+1,j+1}}{z_{i+1,JMAX} - z_{i+1,1}} \tag{69a,b}$$

Ideally, the initial values used should be based on information at stations preceding as well as following the station under consideration. Thus, $\phi_{i,j}$ should be initialized using a suitable weighted combination of relations (68a, 69a) and $z_{i,j}$ using relations (68b, 69b). However, only one of the right-hand quantities would be known in this combination, depending on the direction in which the initialization proceeds with respect to i and j. To maintain the initialization procedure non-iterative, the unknown quantity must be approximated in a suitable manner.

This leads to the following simple expressions, written here for increasing i and j.

$$\frac{\phi_{i,j} - \phi_{i-1,j}}{\phi_{IMAX,j} - \phi_{1,j}} = w_\phi \left[\frac{\phi_{i,j-1} - \phi_{i-1,j-1}}{\phi_{IMAX,j-1} - \phi_{1,j-1}}\right] + (1-w_\phi)\left[\frac{\phi_{i,JMAX} - \phi_{i-1,JMAX}}{\phi_{IMAX,JMAX} - \phi_{1,JMAX}}\right] \tag{70}$$

and

$$\frac{z_{i,j} - z_{i,j-1}}{z_{i,JMAX} - z_{i,1}} = w_z \left[\frac{z_{i-1,j} - z_{i-1,j-1}}{z_{i-1,JMAX} - z_{i-1,1}}\right] + (1-w_z)\left[\frac{z_{IMAX,j} - z_{IMAX,j-1}}{z_{IMAX,JMAX} - z_{IMAX,1}}\right] \tag{71}$$

where

$$w_\phi = \frac{\phi_{i-1,JMAX} - \phi_{i-1,j}}{\phi_{i-1,JMAX} - \phi_{i-1,j-1}} \; ; \quad w_z = \frac{z_{IMAX,j-1} - z_{i,j-1}}{z_{IMAX,j-1} - z_{i-1,j-1}} \; . \tag{72}$$

This procedure has been employed to provide the starting solution for a variety of configurations, in order to test it for versatility. For a configuration involving a simple rectangular domain but requiring non-uniform grid-point distribution, Eqs. (70-72) provide the final solution exactly, consistent with the grid-point distribution specified at the boundaries. Therefore, for this configuration, the converged solution of the transformation equations is obtained in one iteration (Fig. 13).

For a typical turbine-cascade configuration, the starting solution provided by Eqs. (70-72) is shown in Fig. 14a; the corresponding converged solution is shown in Fig. 14b. The striking resemblance between the starting solution and the final solution is responsible for the rapid convergence of the numerical method. In fact, this particular configuration was used as a

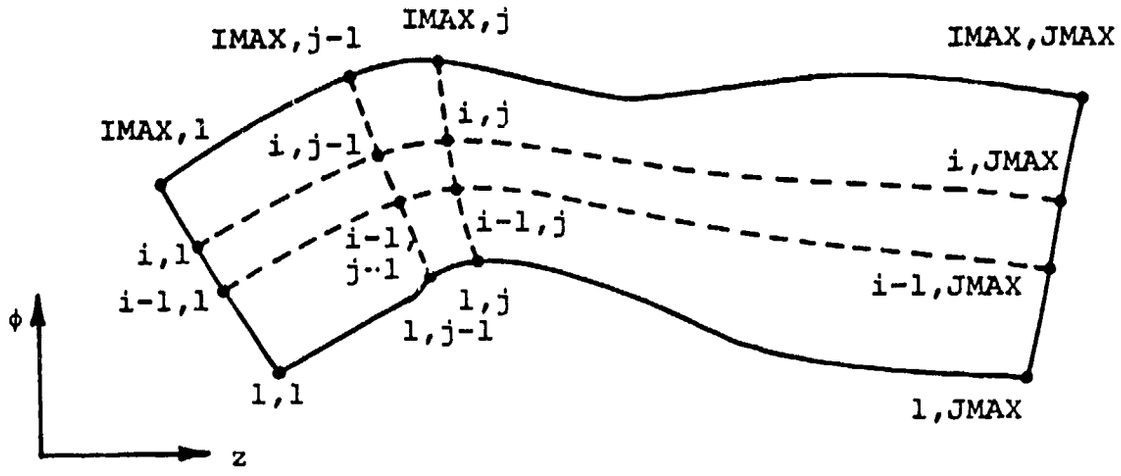

FIG. 12. INITIALIZATION PROCEDURE

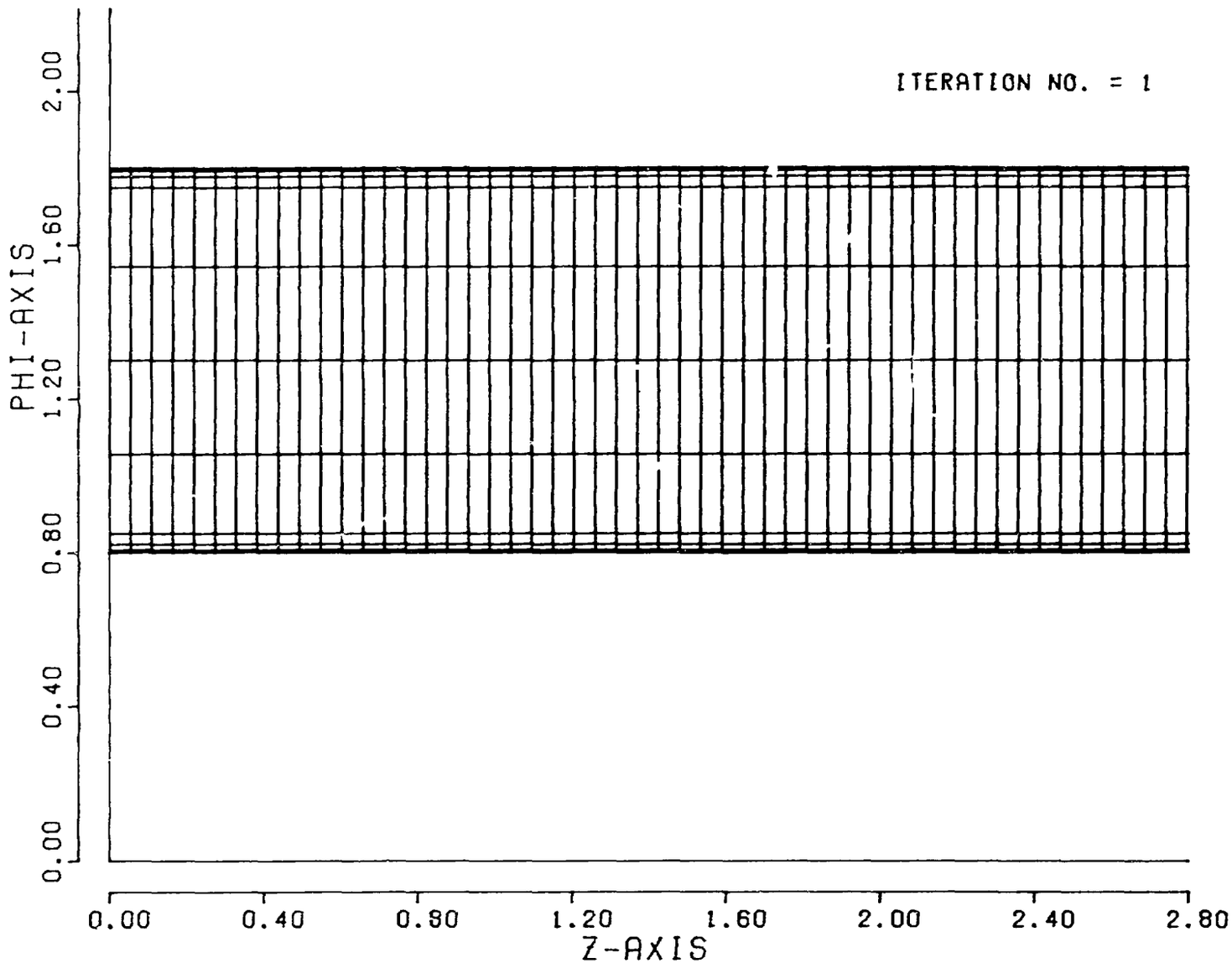

FIG. 13. INITIAL CONDITIONS AND FINAL SOLUTION FOR COORDINATES FOR FLOW THROUGH A STRAIGHT CHANNEL.

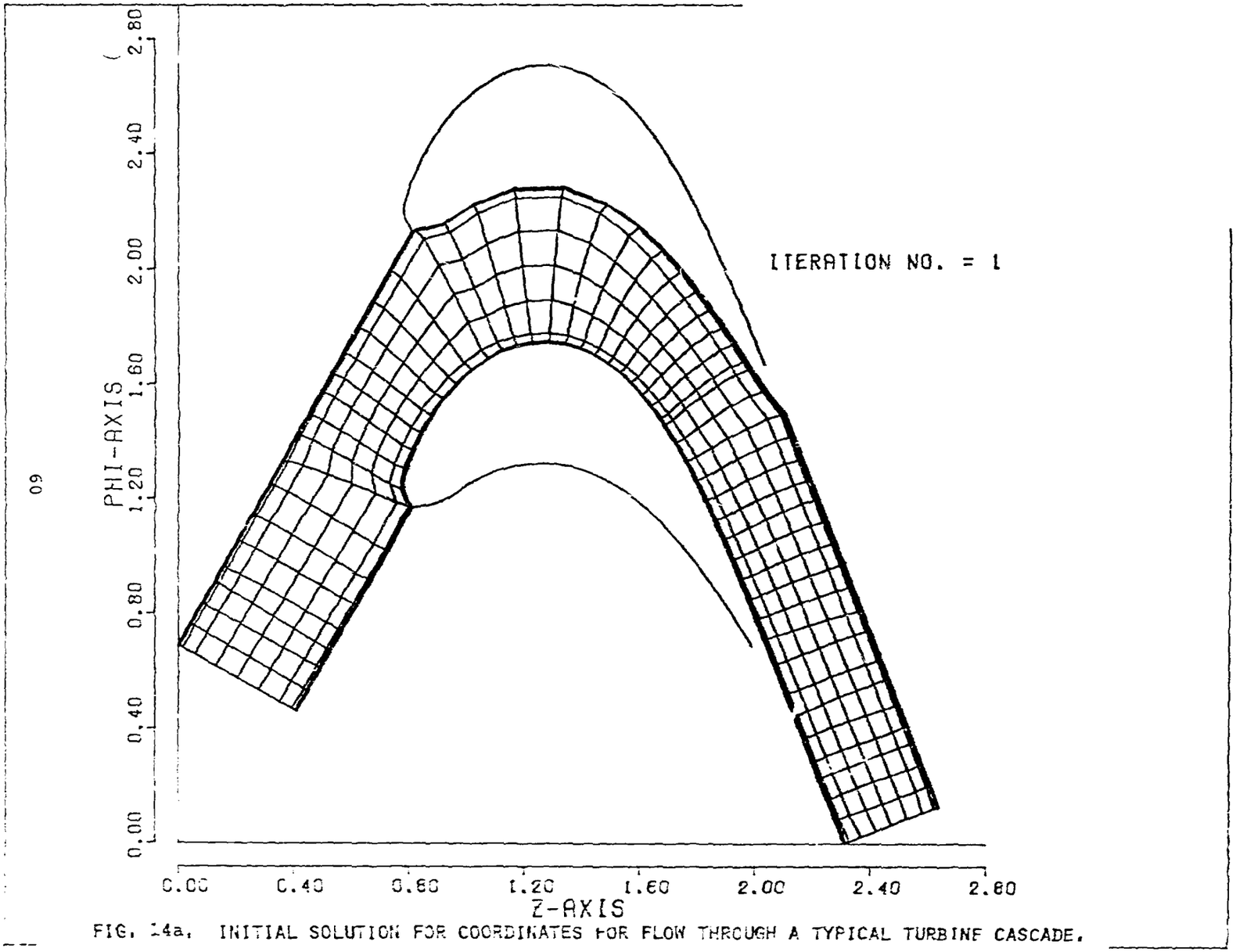

FIG. 14a. INITIAL SOLUTION FOR COORDINATES FOR FLOW THROUGH A TYPICAL TURBINE CASCADE.

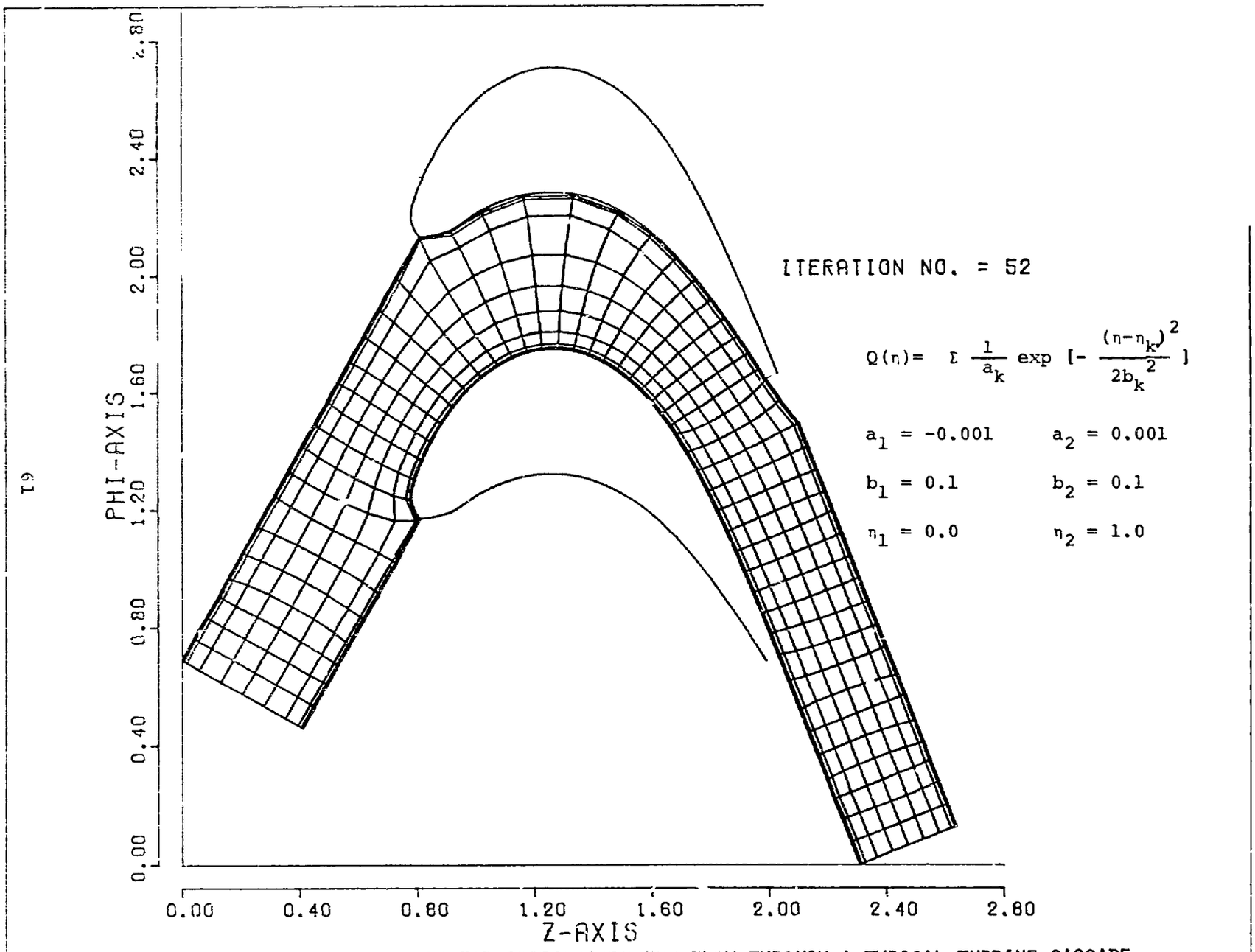

FIG. 14b. CONVERGED SOLUTION FOR COORDINATES FOR FLOW THROUGH A TYPICAL TURBINE CASCADE.

test case to confirm the nonlinear-instability phenomenon caused by large initial errors. With starting conditions consisting of constant values of ϕ and z in the interior, the solution failed to converge.

The usefulness of Eqs. (70-72) for an external flow configuration is indicated in Fig. 15 which shows the starting solution for the coordinates suggested for analyzing the symmetric flow past an airfoil. Other configurations have also been tested by Plant[6].

It is important to note that, in certain limiting situations involving vertical or horizontal straight-line boundaries, care must be taken to avoid possible division by zero in Eqs. (70-72). For example, if the denominators of w_ϕ or w_z vanish, Eq. (72) is appropriately replaced by

$$w_\phi = \frac{JMAX - j}{JMAX - (j-1)} \qquad \text{and} \qquad w_z = \frac{IMAX - i}{IMAX - (i-1)} \quad . \tag{73}$$

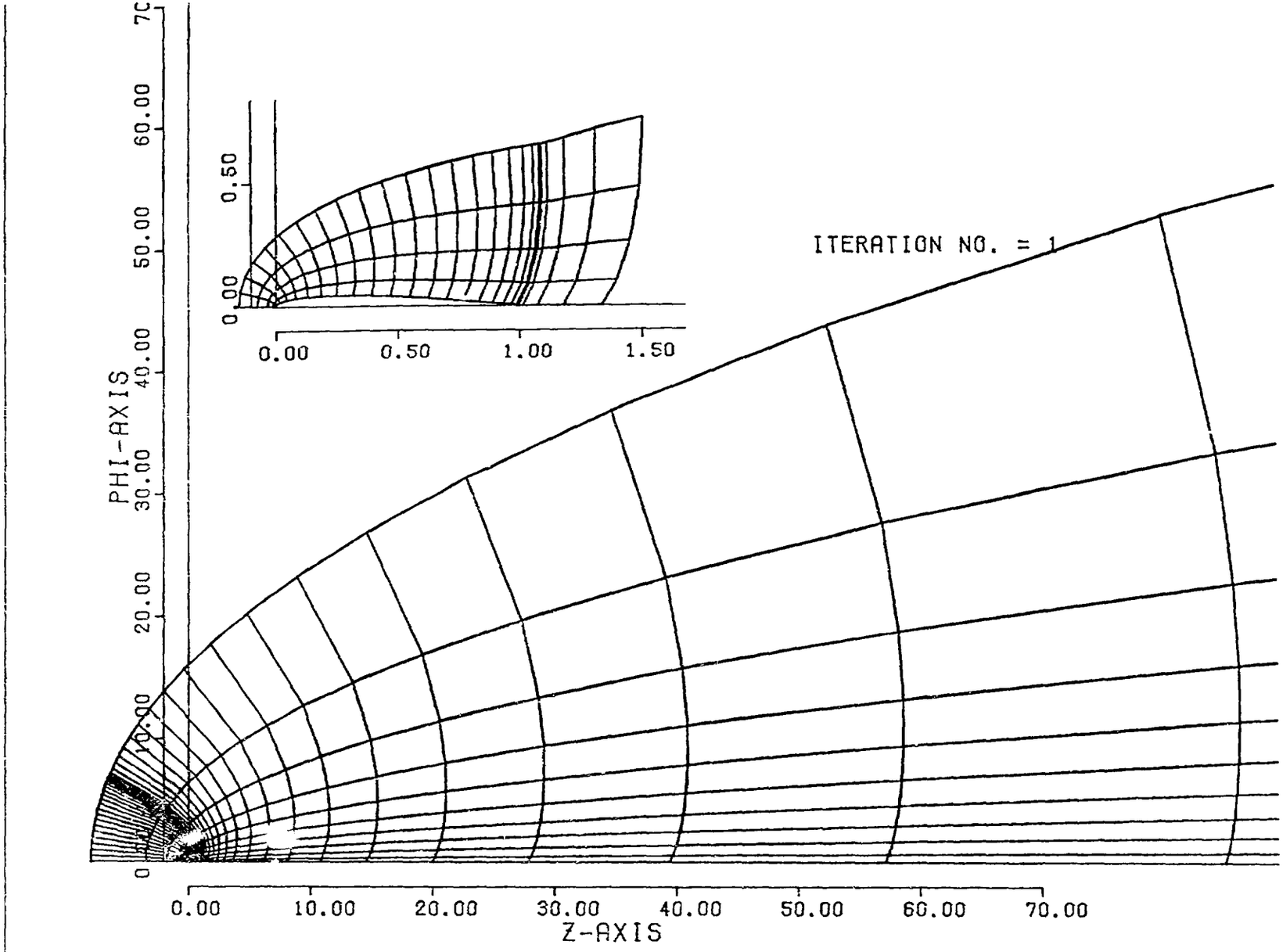

FIG. 15. INITIAL SOLUTION FOR COORDINATES FOR SYMMETRIC FLOW PAST A JOUKOWSKI AIRFOIL.

SECTION V

CONCLUDING REMARKS

In summary, the present study represents a closer analysis of the numerical coordinate-transformation technique and provides important refinements in the procedures involved in determining surface-oriented coordinates for arbitrary geometrical configurations. These refinements lead to a more desirable distribution of mesh points for the finite-difference solution of the corresponding fluid dynamics problem. The resulting procedures are general, are applicable for internal as well as external flow problems and become increasingly useful for high-Re flow calculations. Thus, the study leads to an efficient method for generating suitable surface-oriented coordinates for arbitrary geometries.

Nevertheless, possibilities for further improvement continue to present themselves. For example, even though the coordinate solutions converge quite rapidly for the configurations tested, increased computational efficiency is possible with the use of variable time-steps in the ADI method of solution for the coordinate equations (4-7). Finally, attention is drawn to a concern that arises in the use of a numerical coordinate transformation in the analysis of turbulent flows. Since a numerical mesh-generation procedure represents the body surface by segments of straight lines, the sharp corners formed by these line segments may lead to a distortion, in the resulting turbulent flow solution as compared to the true turbulent flow.

The use of a Schwarz-Christoffel transformation can serve to numerically transform the multi-sided polygon representation of the body surface into a single straight line[17]. Since the Schwarz-Christoffel transformation is a conformal transformation, the resulting coordinates may not, in general, provide appropriate resolution of certain critical regions of the flow. Use of a further numerical transformation may be necessary to achieve the desired resolution.

Finally, it is important to note that the present study has led to significant improvements in the convergence rate of the numerical solutions of the coordinate-transformation equations. Most configurations tested (Fig. 1) required about 20 seconds on a CDC 6600 computer for an (11 x 41) grid to satisfy a convergence criterion of less than one percent change in the relative value of the solution at each grid point, per unit time. The maximum time required for any case tested in this study is about 80 seconds for obtaining a satisfactory coordinate system. These computing times represent an order-of-magnitude reduction in the computer time required prior to the present refinements.

Optimization of the grid-point distribution is necessary in order to reduce truncation errors in the numerical solution, especially in regions where the flow variables undergo large gradients. For complex flows, these regions are not known *a priori*. Adjustment of the grid with the development of the flow field is then necessary. A self-adjusting grid generating procedure is therefore a desirable feature for further study.

APPENDIX A

LOCAL ORTHOGONALITY AND LOCAL CONFORMALITY

This appendix outlines the implications of setting to zero the coefficient b of the mixed-derivative terms in the coordinate equations (4-7), i.e.,

$$\phi_\eta \phi_\zeta + z_\eta z_\zeta = 0 \quad . \tag{A-1}$$

This condition can be rearranged as follows:

$$\left.\frac{\partial \phi}{\partial \eta}\right|_\zeta \left.\frac{\partial \phi}{\partial \zeta}\right|_\eta = - \left.\frac{\partial z}{\partial \eta}\right|_\zeta \left.\frac{\partial z}{\partial \zeta}\right|_\eta$$

or

$$\frac{[\partial \phi/\partial \eta]_\zeta}{[\partial z/\partial \eta]_\zeta} = - \frac{[\partial z/\partial \zeta]_\eta}{[\partial \phi/\partial \zeta]_\eta} \quad . \tag{A-2}$$

Using the chain-rule for differentiation enables rewriting Eq. (A-2) as

$$\left.\frac{\partial \phi}{\partial z}\right|_\zeta = - 1/\left.\frac{\partial \phi}{\partial z}\right|_\eta \quad . \tag{A-3}$$

This clearly implies that the curve ζ=constant is orthogonal to the curve η=constant. Therefore, Eq. (A-1) implies local orthogonality of the (η,ζ) coordinates.

Next, it is shown that the condition for the (η,ζ) coordinates to be conformal is a special case of Eq. (A-1). Since a mapping defined by an analytic function is conformal, $z+i\phi$ and $\zeta+i\eta$ are considered to be complex variables related by an analytic transformation as

$$z + i\phi = f(\zeta+i\eta) \quad . \tag{A-4}$$

Then, by definition of analyticity, the real and imaginary parts of the mapping function satisfy the Cauchy-Riemann conditions, so that

$$z_\zeta = \phi_\eta \quad \text{and} \quad z_\eta = -\phi_\zeta \quad . \tag{A-5}$$

Satisfaction of these conditions implies the satisfaction of condition (A-1), but the converse is not true. Conditions (A-5) place greater restriction on the transformation than does condition (A-1). This can also be seen by observing that conditions (A-5) imply, further, that ϕ and z are harmonic functions satisfying the Laplace equation. In fact, use of conditions (A-5) in Eqs. (6-7) leads to

$$a = c = J \quad \text{and} \quad b = 0 \quad . \tag{A-6}$$

Furthermore, the inverse transformation corresponding to Eq. (A-4) is also analytic and conformal. Therefore, ζ and η satisfy the Cauchy-Riemann equations.

$$\zeta_z = \eta_\phi \quad \text{and} \quad \zeta_\phi = -\eta_z \quad . \tag{A-7}$$

Hence, η and ζ must be harmonic functions, so that the forcing functions Q and R in Eqs. (1-2) must be identically zero. With zero Q and R and with Eqs. (A-6), the inverted coordinate equations (4-5) reduce to simple Laplace equations. This is clearly more restrictive than desired for a general configuration where computational efficiency and accuracy may require a highly non-

uniform mesh-point distribution in the physical plane and, hence, non-zero Q and R in the numerical coordinate-transformation.

APPENDIX B

INVERSION OF EQUATIONS (42a,b)

This appendix presents the details of the derivation of Eqs. (46-47) which represent the inverted forms of the equations

$$\nabla^2_{N,S}\,\eta = Q \quad , \qquad \nabla^2_{N,S}\,\zeta = R \quad , \tag{B-1}$$

where

$$\nabla^2_{N,S} = \frac{1}{h^2}\left[N'^2\,\frac{\partial^2}{\partial N^2} + N''\,\frac{\partial}{\partial N} + S'^2\,\frac{\partial^2}{\partial S^2} + S''\,\frac{\partial}{\partial S}\right] . \tag{B-2}$$

These are Eqs. (42-43) in the text. The symbols used in this appendix have been defined in Section 3.2.1 of the text.

Starting with the functional relationships

$$N = N(\eta,\zeta) \qquad \text{and} \qquad S = S(\eta,\zeta) \tag{B-3}$$

for the numerical coordinate-transformation, the various derivatives appearing in the operator $\nabla^2_{N,S}$ can be expressed in terms of their inverted forms, as follows:

$$\eta_N = S_\zeta/\bar{J} \ , \quad \zeta_N = -S_\eta/\bar{J} \ , \quad \eta_S = -N_\zeta/\bar{J} \ , \quad \zeta_S = N_\eta/\bar{J} \quad , \tag{B-4}$$

$$\eta_{NN} = (N_\zeta A_1 - S_\zeta A_2)/\bar{J} \quad , \quad \zeta_{NN} = (-N_\eta A_1 + S_\eta A_2)/\bar{J} \quad ,$$

$$\eta_{SS} = (N_\zeta B_1 - S_\zeta B_2)/\bar{J} \quad , \quad \zeta_{SS} = (-N_\eta B_1 + S_\eta B_2)/\bar{J} \quad , \tag{B-5}$$

where

$$A_1 = (S_{\eta\eta}S_\zeta^2 + S_{\zeta\zeta}S_\eta^2 - 2S_{\eta\zeta}S_\eta S_\zeta)/\bar{J}^2 \quad ,$$

$$A_2 = (N_{\eta\eta}S_\zeta^2 + N_{\zeta\zeta}S_\eta^2 - 2N_{\eta\zeta}S_\eta S_\zeta)/\bar{J}^2 \quad ,$$

$$B_1 = (S_{\eta\eta}N_\zeta^2 + S_{\zeta\zeta}N_\eta^2 - 2S_{\eta\zeta}N_\eta N_\zeta)/\bar{J}^2 \quad ,$$

$$B_2 = (N_{\eta\eta}N_\zeta^2 + N_{\zeta\zeta}N_\eta^2 - 2N_{\eta\zeta}N_\eta N_\zeta)/\bar{J}^2 \qquad \text{(B-6)}$$

and

$$\bar{J} = N_\eta S_\zeta - N_\zeta S_\eta \quad . \qquad \text{(B-7)}$$

The derivation of Eqs. (B-4 - B-7) parallels that described in Refs. 4 and 5. Substitution of these equations into Eqs. (B-1 - B-2) leads to the two equations given below:

$$N'^2 (N_\zeta A_1 - S_\zeta A_2) + N'' S_\zeta + S'^2 (N_\zeta B_1 - S_\zeta B_2) - S'' N_\zeta = \bar{J}\, h^2 Q$$

and

$$N'^2 (-N_\eta A_1 + S_\eta A_2) - N'' S_\eta + S'^2 (-N_\eta B_1 + S_\eta B_2) + S'' N_\eta = \bar{J}\, h^2 R \quad . \qquad \text{(B-8)}$$

These are rearranged to yield the following form:

$$(N'^2 A_1 + S'^2 B_1 - S'')N_\zeta - (N'^2 A_2 + S'^2 B_2 - N'')S_\zeta = \bar{J}\, h^2 Q$$

and

$$-(N'^2 A_1 + S'^2 B_1 - S'')N_\eta + (N'^2 A_2 + S'^2 B_2 - N'')S_\eta = \bar{J}\, h^2 R \qquad \text{(B-9)}$$

Equations (B-9) can be viewed as two independent equations for the two quantities in parentheses. Therefore, Eqs. (B-9) yield

$$N'^2 A_2 + S'^2 B_2 - N'' = \bar{J}\, h^2 (QN_\eta + RN_\zeta)/(N_\zeta S_\eta - N_\eta S_\zeta) \qquad \text{(B-10)}$$

and

$$N'^2 A_1 + S'^2 B_1 - S'' = \bar{J}\, h^2 (QS_\eta + RS_\zeta)/(N_\zeta S_\eta - N_\eta S_\zeta) \ . \quad \text{(B-11)}$$

Use of Eqs. (B-6 - B-7) in Eqs. (B-10 - B-11) leads to the inverted equations corresponding to Eqs. (B-1 - B-2) as follows:

$$N'^2 (N_{\eta\eta} S_\zeta^2 + N_{\zeta\zeta} S_\eta^2 - 2N_{\eta\zeta} S_\eta S_\zeta) + S'^2 (N_{\eta\eta} N_\zeta^2 + N_{\zeta\zeta} N_\eta^2 - 2N_{\eta\zeta} N_\eta N_\zeta)$$

$$- N'' + \bar{J}^2 h^2 (QN_\eta + RN_\zeta) = 0 \quad \text{(B-12)}$$

and

$$N'^2 (S_{\eta\eta} S_\zeta^2 + S_{\zeta\zeta} S_\eta^2 - 2S_{\eta\zeta} S_\eta S_\zeta) + S'^2 (S_{\eta\eta} N_\zeta^2 + S_{\zeta\zeta} N_\eta^2 - 2S_{\eta\zeta} N_\eta N_\zeta)$$

$$- S'' + \bar{J}^2 h^2 (QS_\eta + RS_\zeta) = 0 \quad \text{(B-13)}$$

The inverted equations (46a,b) in the text are simply a rearranged form of Eqs. (B-12 - B-13) as

$$\bar{a}\, N_{\eta\eta} + 2\bar{b}\, N_{\eta\zeta} + \bar{c}\, N_{\zeta\zeta} - N'' + h^2 \bar{J}^2 (QN_\eta + RN_\zeta) = 0 \quad \text{(B-14)}$$

and

$$\bar{a}\, S_{\eta\eta} + 2\bar{b}\, S_{\eta\zeta} + \bar{c}\, S_{\zeta\zeta} - S'' + h^2 \bar{J}^2 (QS_\eta + RS_\zeta) = 0 \quad \text{(B-15)}$$

where $\bar{a}$, $\bar{b}$, $\bar{c}$ are as defined in Eq. (47) in the text.

REFERENCES

1. Ives, D.C., "A Modern Look at Conformal Mapping, Including Doubly Connected Regions," AIAA Paper No. 75-842, presented at the AIAA 8th Fluid and Plasma Dynamics Conference, Hartford, Connecticut, June, 1975.
2. Grossman, B. and Melnik, R.E., "The Numerical Computation of the Transonic Flow Over Two-Element Airfoil Systems," Lecture Notes in Physics, Vol. 59, Springer Verlag, 1976.
3. Moretti, G., "Conformal Mappings for Computations of Steady, Three-Dimensional, Supersonic Flows," Numerical/Laboratory Computer Methods in Fluid Mechanics, Editor: A.A. Pouring, ASME Publication, 1976.
4. Thompson, J.F., Thames, F.C. and Mastin, C.W., "Automatic Numerical Generation of Body-Fitted Curvilinear Coordinate Systems for Field Containing Any Number of Arbitrary Two-Dimensional Bodies," Journal of Computational Physics, Vol. 15, 1974, p. 299.
5. Ghia, U. and Ghia, K.N., "Numerical Generation of a System of Curvilinear Coordinates for Turbine Cascade Flow Analysis," University of Cincinnati Report No. AFL 75-4-17, 1975.
6. Plant, T., Private Communication, Air Force Flight Dynamics Laboratory, Dayton, Ohio.
7. Roache, P.J., "Computational Fluid Dynamics," Hermosa Publishers, 1976.
8. Warsi, Z.A.U. and Thompson, J.F., "Machine Solutions of Partial Differential Equations in the Numerically Generated Coordinate Systems," Engineering and Industrial Research Station, Mississippi State University Report No. MSSUEIRS-ASE-77-1, August 1976.
9. Thompson, J.F. and Thames, F.C., "Numerical Solution of Potential Flow About Arbitrary Two-Dimensional Multiple Bodies," to appear as NASA Contractor's Report.
10. Ghia, U., Ghia, K.N., and Studerus, C.J., "A Study of Three-Dimensional Laminar Incompressible Flow in Ducts," to appear in International Journal of Computers and Fluids, 1977.

11. Mitchell, A.R., Computational Methods in Partial Differential Equations, John Wiley and Sons, 1969.

12. Greenspan, D. and Jain, P.C., "On Non-Negative Difference Analogues of Elliptic Differential Equations," Tech. Report 490, Mathematics Research Center, Madison, Wisconsin, 1964.

13. Potter, D.E. and Tuttle, G.H., "The Construction of Discrete Orthogonal Grids," Journal of Computational Physics, Vol. 13, 1973, pp. 483-501.

14. Ghia, K.N., "Streamwise Flow Along an Unbounded Corner," AIAA Journal, Vol. 13, No. 7, July 1975, pp. 902-907.

15. Davis, R.T., "Numerical Solution of the Navier-Stokes Equations For Symmetric Laminar Incompressible Flow Past a Parabola," Journal of Fluid Mechanics, Vol. 51, Pt. 3, 1972, pp. 417-433.

16. Mikhail, A.G. and Ghia, K.N., "Study of Compressible Flow Along an Axial Corner," AIAA Paper No. 77-685, presented at the AIAA 10th Fluid and Plasma Dynamics Conference, Albuquerque, New Mexico, June, 1977.

17. Anderson, O.L., "User's Manual for a Finite-Difference Calculation of Turbulent Swirling Compressible Flow in Axisymmetric Ducts with Struts and Slot-Cooled Walls," USAAMRDL-TR-74-50, U.S. Army Air Mobility Research and Development Laboratory, Virginia.

☆U.S.Government Printing Office: 1978 — 757-080/428